

**ECONOMIC GEOLOGY
RESEARCH UNIT**

University of the Witwatersrand
Johannesburg

**THE NATURE OF GOLD MINERALIZATION IN THE
SABIE-PILGRIM'S REST GOLDFIELD,
EASTERN TRANSVAAL, SOUTH AFRICA**

**R.H. BOER, F.M. MEYER, L.J. ROBB,
J.R. GRANEY and T.W. VENNEMANN**

• **INFORMATION CIRCULAR No. 262**

UNIVERSITY OF THE WITWATERSRAND
JOHANNESBURG

**THE NATURE OF GOLD MINERALIZATION IN THE
SABIE-PILGRIM'S REST GOLDFIELD,
EASTERN TRANSVAAL, SOUTH AFRICA**

by

**R.H. BOER¹, F.M. MEYER², L.J. ROBB²,
J.R. GRANEY³ and T.W. VENNEMANN³**

(¹ *Economic Geology Research Unit, ² Department of Geology,
University of the Witwatersrand, Private Bag 3, P.O. WITS 2050,
South Africa and ³ Department of Geological Sciences,
University of Michigan, Ann Arbor, Michigan 48019,
U.S.A.)*

**ECONOMIC GEOLOGY RESEARCH UNIT
INFORMATION CIRCULAR No. 262**

April, 1993

**THE NATURE OF GOLD MINERALIZATION IN THE
SABIE - PILGRIM'S REST GOLDFIELD, EASTERN TRANSVAAL,
SOUTH AFRICA**

ABSTRACT

New geochemical data obtained from fluid inclusion, as well as whole rock, light stable isotope and inclusion fluid gas analyses provide evidence of the temperature, composition and sources of hydrothermal fluids associated with the formation of the Sabie-Pilgrim's Rest Goldfield. Gold mineralization is epigenetic and confined to transgressive, vertical reefs, stratabound flat reefs, as well as sill/dyke-associated quartz-carbonate reefs. Reef-forming fluids were focused into permeable northeasterly trending lineaments and averted along low angle, bedding parallel, simple shear thrusts. The lower age limit of gold mineralization (2027 ± 31 Ma; initial $^{87}\text{Sr}/^{86}\text{Sr}$ ratio = 0.70416) corresponds well with the emplacement age of the mafic phase of the Bushveld Complex. Textural relationships among reef-filling minerals indicated that chalcopyrite, bismuth, bismuth sulphosalts, fahlores and native gold precipitated last as fracture-fillings in pyrite. Fluid inclusion petrography revealed the presence of the following types of inclusions: Type 1 - H_2O -carbonic with the occasional daughter crystal; Type 2 - high salinity H_2O -carbonic inclusions with multiple daughter crystals; and Type 3 - low salinity late-stage aqueous inclusions often occurring without a vapour bubble. The nature of the ore-bearing fluid in the Sabie-Pilgrim's Rest Goldfield was predominantly aqueous with less than 5 mole% consisting of mainly carbonic species, sulphur components and nitrogen. On the basis of relative N_2 , Ar and CO_2 contents, large scale fluid interaction with air saturated meteoric water is ruled out. Oxygen isotope values of quartz from the vertical reefs yielded an average $\delta^{18}\text{O}$ value of 14.2 ‰, an average $\delta^{18}\text{O}$ value of 16.1 ‰ was obtained for the flat reefs, while the sill/dyke associated deposits showed an average $\delta^{18}\text{O}$ value of 20.7 ‰. ^{18}O content progressively decreases with increasing depth and the $\delta^{18}\text{O}$ values in individual reef systems are remarkably homogeneous. $\delta^{34}\text{S}$ values of reef pyrite range from -2.8 to +3.1 ‰. δD , $\delta^{18}\text{O}$ and $\delta^{13}\text{C}$ values from inclusion fluids ($\delta\text{D} = -37$ to -67 ‰; $\delta^{18}\text{O} = +6.5$ to +15.4 ‰; $\delta^{13}\text{C} = -11.7$ to -1.4 ‰) coincide predominantly with values of primary magmatic water. Interaction of the ore fluid with the host rocks was of limited extent such that the magmatic isotopic and gas chemistry signature of the fluids remains clear. This limited interaction places constraints on the possible sources of gold - a magmatic source, rather than a remobilized sedimentary source being favoured. Mineralization occurred at temperatures around 320°C , at pressures in the range 2.2 to 2.5 kb and at depths of 7 to 8 km. Ore-bearing fluids were probably derived from a deep seated portion of the granitic phase of the Bushveld Complex.

____oo____

**THE NATURE OF GOLD MINERALIZATION IN THE
SABIE - PILGRIM'S REST GOLDFIELD, EASTERN TRANSVAAL,
SOUTH AFRICA**

CONTENTS

	Page
INTRODUCTION	1
GEOLOGICAL RELATIONSHIPS	2
Geological setting	2
Age of gold mineralization	3
MINERALOGY	5
FLUID INCLUSIONS DATA	7
Description of fluid inclusions	7
Type 1 inclusions	7
Type 2 inclusions	9
Type 3 inclusions	9
Quadrupole mass spectrometer gas analyses	10
LIGHT STABLE ISOTOPE RELATIONSHIPS	13
Quartz oxygen isotopic data	13
Pyrite sulphur isotopic data	15
Fluid inclusion stable isotopic data	15
DISCUSSION	17
Temperature, pressure and fluid composition	17
Gold solubility and depositional mechanisms	20
A GENETIC MODEL FOR THE SABIE - PILGRIM'S REST GOLDFIELD	21
CONCLUSIONS	23
ACKNOWLEDGEMENTS	24
REFERENCES	24

 oOo

Published by the Economic Geology Research Unit
Department of Geology
University of the Witwatersrand
1 Jan Smuts Avenue, Johannesburg 2001
South Africa
ISBN 1 86838 058 1

THE NATURE OF GOLD MINERALIZATION IN THE SABIE - PILGRIM'S REST GOLDFIELD, EASTERN TRANSVAAL, SOUTH AFRICA

INTRODUCTION

This study presents an evaluation of newly acquired fluid inclusion, as well as whole rock, light stable isotope and inclusion fluid gas analyses. The aim of this paper is to discuss the nature of gold mineralization and to provide quantitative information on the fluids associated with mineralization in the Sabie-Pilgrim's Rest Goldfield. To this end the writers have selected samples representative of the various gold deposits found throughout the stratigraphy. Temperature, composition and stable isotopic data from fluid inclusions in quartz carbonate reefs, as well as stable isotopic data from quartz and pyrite, were used to specify pressure, temperature, fO_2 and aH_2S conditions under which mineralization occurred.

The Sabie-Pilgrim's Rest Goldfield lies along the edge of the Transvaal Drakensberg escarpment in the eastern Transvaal. Small alluvial placer gold occurrences led to the discovery of the Goldfield in 1873. Gold mineralization in this, the third largest gold-source in South Africa, is epigenetic and confined to transgressive, vertical reefs¹, stratabound flat reefs, as well as sill/dyke-associated quartz-carbonate reefs. The stratabound reefs are composed of multiple sheets of quartz-carbonate, usually associated with thin slivers of carbonaceous shale host rock. Anhedral buck quartz, similar to that described by Dowling and Morrison (1989), comprise the bulk of the reefs. Small vugs lined with euhedral crystals of quartz are found locally. The average thickness of the horizontal reefs ranges between 5 - 40 cm. Massive quartz blows, stockworks, and breccias, consisting of a mixture of reef material and host-rock fragments, are locally abundant and economically significant. Surrounding such zones of reef thickening (commonly up to 3m) are subparallel stringer veins, which are locally mineralized, and occasional subvertical stringer veins. These stringers pinch-out within tens of centimetres from the main reef component. The gold grade is highly variable (from traces to over 60 g/t), with the overall grade in the order of 5.4 g/t Au (A.R.C. Fowler, pers. comm. 1993; Boer, 1993). In most deposits there are gradational differences in gold grade along strike such that alternations between ore-grade zones and low-grade waste zones can be distinguished. This situation gives rise to a characteristic ore-shoot pattern (Wybergh, 1925; Zietsman, 1967), with little evidence of mineralogical or elemental zoning present.

Wall-rock alteration associated with emplacement of the quartz reefs is limited in extent, and vein selvaging has played a major role in controlling fluid/mineral interaction. Within the surrounding shales, a well-developed subhorizontal planar fabric, comprising a closely spaced cleavage, is developed. Cleavage surfaces often bear slickensides as evidence of early faulting and fine-grained euhedral pyrite occurs as fabric-parallel layers within the shales (Harley and Charlesworth, 1992). Mineralogically, the shale horizons are mainly composed of sericite with minor amounts of quartz and organic carbon.

¹Within the Sabie-Pilgrim's Rest Goldfield, individual ore bodies or lodes are locally referred to as "reefs" (c.f. Witwatersrand conglomerate hosted ore deposits). This usage is followed in the paper with a reef being defined as a quartz-carbonate-sulphide-gold vein deposit.

A prominent series of northeasterly trending lineaments are evident within the Goldfield. Mafic dyke emplacement, post-mineralization normal faulting, and limited graben development have occurred parallel to this trend. Bedding in the Goldfield dips between 4° and 15° to the west. Reef emplacement is controlled by low angle ($\sigma_1 \leq 5^{\circ}$) southeastward verging bedding-parallel simple shear thrusts (Harley and Charlesworth, 1992). Small-scale duplexes and shallowly westward-dipping ramp structures as well as asymmetric folds, are typically developed within the mineralized carbonaceous shale.

GEOLOGICAL RELATIONSHIPS

Geological setting

In the Sabie-Pilgrim's Rest area (Fig. 1), the protobasinal Wolkberg Group forms the lowermost part of the Proterozoic Transvaal Sequence and lies unconformably on the

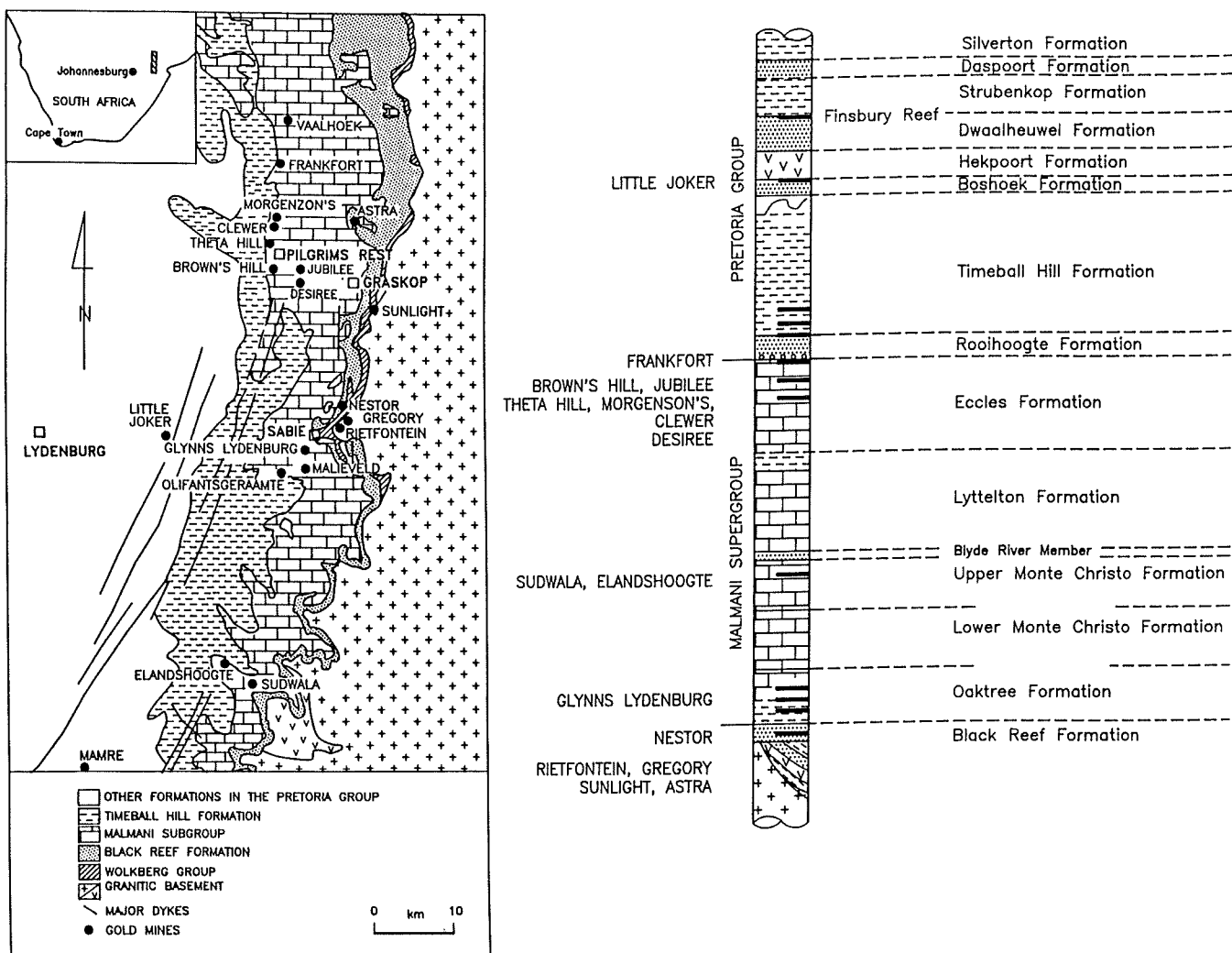


Figure 1: Geological map of the Sabie-Pilgrim's Rest Goldfield with schematic stratigraphic column. Positions of mines are indicated (modified after Harley and Charlesworth, 1992, 1993).

Archaean Nelspruit batholith. The latter comprises a large, composite body of granodiorite-adamellite (Robb *et al.*, 1983). Disconformably overlying the Wolkberg Group, are the siliciclastic sedimentary rocks of the Black Reef Formation which forms the top of the main escarpment in the area. The Black Reef Formation consists of feldspathic quartzite with interlayered lenses of grit and conglomerate. The Malmani Subgroup (part of the Chuniespoort Group) conformably overlies the Black Reef Formation. The Malmani Subgroup consists of the Oaktree, Monte Christo, Lyttelton and Eccles Formations and is host to the majority of gold-bearing quartz reefs. Formational divisions within the Malmani Subgroup are based mainly on the variations in the chert content and type of algal structures found in the dolomite (Button, 1973; Clendenin, 1989). The Oaktree Formation is comprised of iron- and manganese-rich dolomite, carbonaceous shale, and quartzite, whereas the Monte Christo Formation is characterised by a widely developed sequence of oolitic carbonate rocks (Button, 1986). Siliciclastic sediments (quartzite and/or shale) mark the base of the overlying chert-poor Lyttelton Formation, which is composed mainly of dark-coloured quartz-arenite in the Sabie-Pilgrim's Rest area (Tyler, 1989). This unit grades upward to the upper dolomite and chert zone of the Eccles Formation. Following the deposition of these sediments, the strata were exposed and an extensive erosional period ensued. This resulted in the formation of a widely developed chert breccia and chert pebble conglomerate at the base of the siliciclastic dominated Pretoria Group, the so-called Bevets Conglomerate. The Pretoria Group consists of alternating shale and quartz-arenites, with minor conglomerates, granulestones and interlayered volcanic units (Button, 1973). The succession, as developed in the eastern Transvaal, is approximately 7000-8000 m in thickness (Button, 1986).

A large number of basic sills, of different ages, have intruded into the Transvaal Sequence in the Sabie-Pilgrim's Rest area. The majority of these sills are probably related to the Bushveld Complex and increase in frequency upwards in the stratigraphy (Sharpe, 1984). The Transvaal Sequence sediments and volcanic rocks are metamorphosed, both by the intrusive sills and by the Bushveld Complex. The metamorphic effects of the Bushveld Complex transgress the stratigraphy and extend down to the Malmani Subgroup in places (Button, 1986).

Age of gold mineralization

Determination of the age of mineralization in the Goldfield presents problems due to the lack of suitable datable ore-stage material. However, age constraints can be placed on the sedimentation of the Transvaal Supergroup (e.g. by the pre-Transvaal acid lavas from the Dennilton area that yielded an age of 2460 ± 12 Ma, Coertze *et al.*, 1978). Furthermore, Jahn *et al.* (1990) established an age of 2557 ± 49 Ma for the stromatolitic dolomites of the Schmidtsdrift Formation in the Griqualand West basin, which is a facies equivalent of the Malmani Subgroup in the Transvaal (Beukes, 1973). In addition, Beukes and Klein (1990) have suggested that deposition of the Transvaal Sequence commenced at approximately 2500 Ma, based on sedimentological evidence. The upper age limit to Transvaal sedimentation is indicated by Rb/Sr whole rock data of 2070 ± 90 Ma from basalts of the Olifantshoek Group, which overlie the Transvaal Sequence in the northern Cape Province (Crampton, 1974).

The uppermost stratigraphic limit of Pilgrim's Rest gold mineralization (the Finsbury Reef) occurs at the contact of the Strubenkop and the Dwaalheuwel Formations of the Pretoria Group. The underlying Hekpoort Formation has been dated at 2224 ± 21 Ma (Burger and Coertze, 1975), and establishes a lower limit on the age of quartz-reef gold mineralization. At the Olifantsgeraamte Mine, near Sabie, a metamorphosed diabase sill is intersected by an auriferous quartz reef associated with pronounced wall-rock alteration (Fig. 2a). Rubidium and strontium abundances and isotopic compositions of metamorphosed and altered dolerite samples were analyzed, following the procedure described by Potts (1987), and are indicated in Table 1 and Figure 2b. Samples affected by the reef-associated alteration are randomly distributed on Figure 2b, and were therefore not used in calculating an isochron. However, the Rb-Sr isotopic ratios of the metamorphosed dolerite samples, not affected by the reef-associated alteration, yield an errorchron corresponding to an age of 2027 ± 39 Ma with an initial $^{87}\text{Sr}/^{86}\text{Sr}$ ratio of 0.704163 ± 0.000311 (MSWD = 15.523).

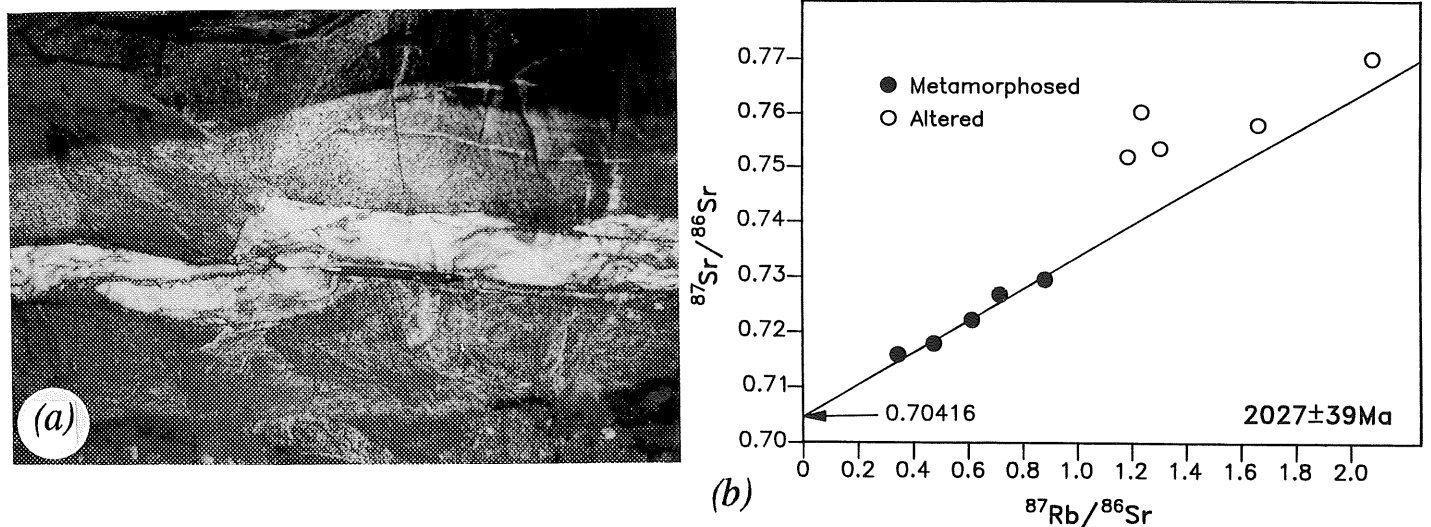


Figure 2: (a) Underground exposure at the Olifantsgeraamte Mine, near Sabie, of an auriferous quartz vein, associated with a pronounced alteration halo, cross-cutting a dolerite sill. (b) Rb-Sr errorchron of unaltered whole rock dolerite samples shown in (a). The errorchron gives an age of 2027 ± 39 Ma with an initial $^{87}\text{Sr}/^{86}\text{Sr}$ of 0.70416 (MSWD = 15.5). The Rb-Sr ratios of altered samples have been completely reset.

This age is considered to represent the timing of metamorphism of the dolerite sill, brought about by emplacement of the mafic phase of the Bushveld Complex, which has been dated at 2061 ± 27 Ma (Walraven *et al.*, 1990). Interpretation of the Rb-Sr data for both altered and metamorphosed samples clearly show that gold-reef associated alteration overprints the metamorphism, disturbing the metamorphic errorchron. This dictates that mineralization post-dates metamorphism, and by implication the mafic phase of the Bushveld Complex. The metamorphic age thus represents a lower age limit for Pilgrim's Rest-type gold mineralization. Gold mineralization is probably related to the granitic phase of the Bushveld Complex, which was emplaced later and is therefore younger than the mafic layered rocks (Walraven, 1988).

Table 1. Composition of quartz-hosted inclusion fluids in mole % as determined by quadrupole mass spectrometer gas analyses. Abbreviations for the different localities are as follow: AST - Astra; CLW - Clewer West; FKM - Frankfort; GLS - Glyns Lydenburg Sheba; GRR - Gregory; JBH - Jubilee; LJM - Little Joker; MGL - Morgenzon; NSM - Nestor; OGM - Olifantsgeraante; SUD - Sudwala; SUN - Sunlight; VLH - Vaalhoek. Exact localities within the Goldfield of BM & S samples are unknown

Sample	H ₂ O	CO ₂	CH ₄	C ₂ H ₆	N ₂	Ar	H ₂ S	SO ₂	HCl	Total
AST109	96.641	3.216	0.078	0.000	0.0000	0.0065	0.0043	0.0007	0.0520	99.998
BM184A	99.538	0.249	0.053	0.069	0.0000	0.0067	0.0170	0.0091	0.0560	99.998
BM184B	99.744	0.127	0.050	0.008	0.0169	0.0019	0.0074	0.0019	0.0430	100.000
BM7384	98.635	1.088	0.157	0.008	0.0138	0.0009	0.0250	0.0005	0.0720	99.999
CLW016	96.969	2.814	0.128	0.017	0.0235	0.0021	0.0047	0.0020	0.0370	99.998
SUD211	99.010	0.758	0.029	0.047	0.0805	0.0041	0.0045	0.0019	0.0650	99.999
FKM075B	84.634	14.930	0.394	0.007	0.0000	0.0009	0.0089	0.0029	0.0120	99.990
FKM076B	94.374	5.363	0.214	0.015	0.0000	0.0026	0.0043	0.0026	0.0210	99.997
GLS052	94.67	5.210	0.046	0.009	0.0181	0.0040	0.0059	0.0015	0.0310	99.996
GRR300	99.482	0.330	0.079	0.021	0.0251	0.0085	0.0085	0.0025	0.0430	99.999
JBH043	89.518	10.313	0.114	0.011	0.0000	0.0020	0.0051	0.0010	0.0290	99.993
LJM090	93.792	5.951	0.178	0.025	0.0000	0.0000	0.0045	0.0007	0.0330	99.984
MGL204	98.824	0.992	0.043	0.079	0.0000	0.0017	0.0050	0.0031	0.0520	99.999
NSM093	99.340	0.529	0.053	0.019	0.0000	0.0048	0.0031	0.0006	0.0500	100.000
NSM098	88.794	10.534	0.561	0.023	0.0000	0.0077	0.0069	0.0024	0.0620	99.991
OGM078	98.491	1.147	0.081	0.074	0.1067	0.0108	0.0140	0.0027	0.0710	99.998
S1017	97.453	2.380	0.081	0.007	0.0181	0.0039	0.0055	0.0012	0.0480	99.998
SUN003	99.150	0.733	0.031	0.019	0.0000	0.0036	0.0032	0.0002	0.0590	100.000
VLH040A	97.421	2.521	0.025	0.009	0.0000	0.0024	0.0041	0.0022	0.0130	99.998
VLH040B	93.265	6.607	0.021	0.014	0.0481	0.0036	0.0055	0.0017	0.0290	99.995

MINERALOGY

The gangue within the reefs is overwhelmingly dominated by quartz (Fig. 3a), with lesser amounts of ferruginous carbonates and sporadic occurrences of muscovite, scheelite and rare rutile. Such gangue mineralogy is typical of what may be expected in a selvaged reef with a high fluid/rock ratio (Cathles, 1991). Inclusions of dolomitic and graphitic wall rock material are common and give rise to the sheeted (ribbon textured) nature of these reefs (Fig. 3b). Pyrite is the dominant sulphide, with varying amounts of arsenopyrite, fahlores (tetrahedrite-tennantite), chalcopyrite, bismuth sulphosalts, bismuth and pyrrhotite. Other ore minerals that were recognized in small quantities include galena, bornite and sphalerite (Swiegers, 1949), as well as stannite and native indium (P.H. Bentley pers. comm. 1992). The sulphide mineralogy of the vertical reefs, the stratabound reefs and the sill/dyke associated deposits is very similar. In addition, the modal proportions of sulphide minerals varies to a very limited extent between the various localities as well as within portions of a single orebody. No distinct zonation patterns of hypogene ore mineral assemblages have been observed amongst the various reefs, or even within one particular reef unit. The distribution of the ore minerals in the Goldfield suggests that the horizontal reefs associated with the Oaktree Formation as well as the upper Lyttleton and Eccles Formations are characterized by a more complex suite of ore minerals (i.e. pyrite, arsenopyrite, fahlores, chalcopyrite, bismuth sulphosalts, bismuth and pyrrhotite), whereas the flat reefs occurring at intermediate stratigraphic positions, i.e. Monte Christo and lower Lyttleton Formations, as well as those deposits associated with diabase intrusives, contain predominantly pyrite and lesser amounts of chalcopyrite and sphalerite.

Despite limited variations in the modal proportions amongst the various localities, a strikingly consistent paragenesis has been recognized. Three stages of sulphide mineralization have been identified: (1) early pyrites from the wall rock associated with the gold mineralized reefs are euhedral to subhedral in form and are virtually free from inclusions of other minerals, apart from a few included gold grains; (2) a second stage of mineralization is indicated by coarser-grained pyrites containing inclusions of chalcopyrite and gold. Contemporaneously or slightly later, arsenopyrite was formed which also contains inclusions of chalcopyrite and tetrahedrite and, in places, overgrows and replaces pyrite. This mineralization episode was accompanied by quartz and carbonate gangue deposition; and (3) following the second stage of mineralization was a period of brittle deformation of the ore bodies, as indicated by the abundant fractures in pyrite and arsenopyrite and also by clasts of wall-rock material found enclosed within quartz in the ore zones. These fractures and intergranular spaces in the early sulphide assemblage were filled by a later suite of fahlores, chalcopyrite, bismuth sulphosalts, native bismuth and gold as well as accompanying gangue. There is a distinct increase in gold content towards the later stages of sulphide mineralization, with the majority of gold being emplaced at a very late stage. The history of the ore-forming processes in sill/dyke associated deposits, i.e. the Olifantsgeraamte and Vaalhoek Mines, seems to be less complex. It appears that only one generation of pyrite and chalcopyrite was developed, and this suite of minerals also contains the gold, which typically occurs as round inclusions.

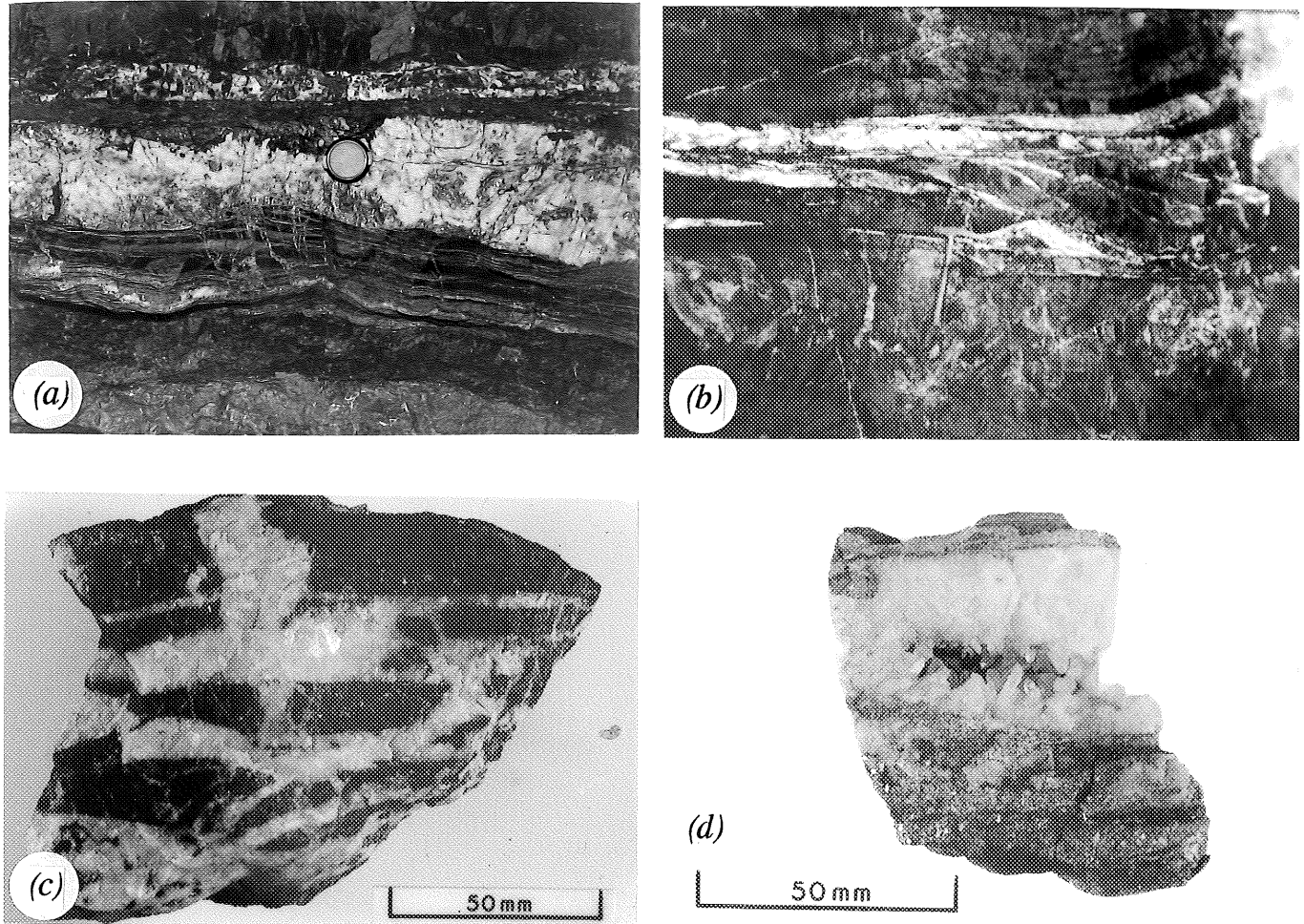


Figure 3: Underground exposure of gold-bearing reef. (a). Typical quartz-carbonate reef with abundant coarse-grained pyrite, Elandshoogte Mine. (b). Sheeted appearance (ribbon texture) of reef with graphic and dolomitic wall-rock inclusions, Glynns-Lydenburg Mine, Sheba Section. (c). Quartz-cemented breccias, Elandshoogte Mine. (d). Comb quartz, Clewer Mine.

Quantitative electron microprobe (EMP) analyses of the bismuth sulphosalts indicate that their composition falls within the aikinite ($PbCuBiS_3$) - bismuthinite (Bi_2S_3) solid solution series (Boer, 1993). Notably, it was Swiegers (1949) who first recognized Pb-rich bismuth sulphosalts in the Sabie-Pilgrim's Rest Goldfield. Sulphide minerals in the Goldfield are homogeneous and do not show elemental zonation, except for arsenic zonation in euhedral pyrite grains. The size of the gold grains, occurring as fracture fillings in pyrite, vary from $< 5 \mu m$ to $\pm 80 \mu m$, while the average size was in the order of 20 to $25 \mu m$. This was consistent for the different modes of gold occurrences described above, although nuggets as large as 3.7 kg have been reportedly found in the alluvial deposits by early prospectors. Despite a measure of overlap in fineness, the average values show an increase in silver content as the associated sulphide mineral paragenesis becomes more complex (Boer, 1993). No relationship exists between the size or the stratigraphic position of the gold grains and their chemistry.

FLUID INCLUSION DATA

Description of fluid inclusions

Fluid inclusion data were obtained by microthermometric heating and freezing, using the standard technique described by Roedder (1984). Temperatures of phase changes were obtained with a FLUID INC. adapted U S Geological Survey heating-freezing system, and the thermocouple was calibrated against synthetic fluid inclusions (Sterner and Bodnar, 1984). Microthermometric measurements were made on inclusions that could be confidently classified and were large enough to permit easy observations of phase changes.

All of the quartz reefs examined experienced repeated fracturing in the presence of aqueous fluids as evidenced by abundant planes of secondary inclusions observed at low magnification. Generally, the high density of randomly oriented fractures decorated with fluid inclusions made it difficult to determine with confidence whether a given inclusion was along one of these fractures or was trapped during crystal growth. For this reason, the authors have not attempted to classify the fluid inclusion types according to the criteria of Roedder (1984), but rather have related groups of inclusions to various stages of reef filling. Two optically distinct varieties of quartz were observed, namely an early, grey to milky translucent variety and a later transparent type which either engulfs or occurs along microfractures in the milky quartz with distinctly different types of fluid inclusions. In all of the samples studied from the horizontal reefs, approximately 95 % of the reef-filling quartz is of the early, milky variety. When quartz specimens are examined microscopically, any given field of view generally contains a number of the types of fluid inclusions described below, the latter "coexisting" with one another. The fluid inclusions occurring in quartz may be classified as follows.

Type 1 inclusions

Three phases, an aqueous liquid, a carbonic liquid, and a vapour bubble, are visible at room temperatures (Fig. 4a). Daughter crystals are occasionally present. The liquid-to-

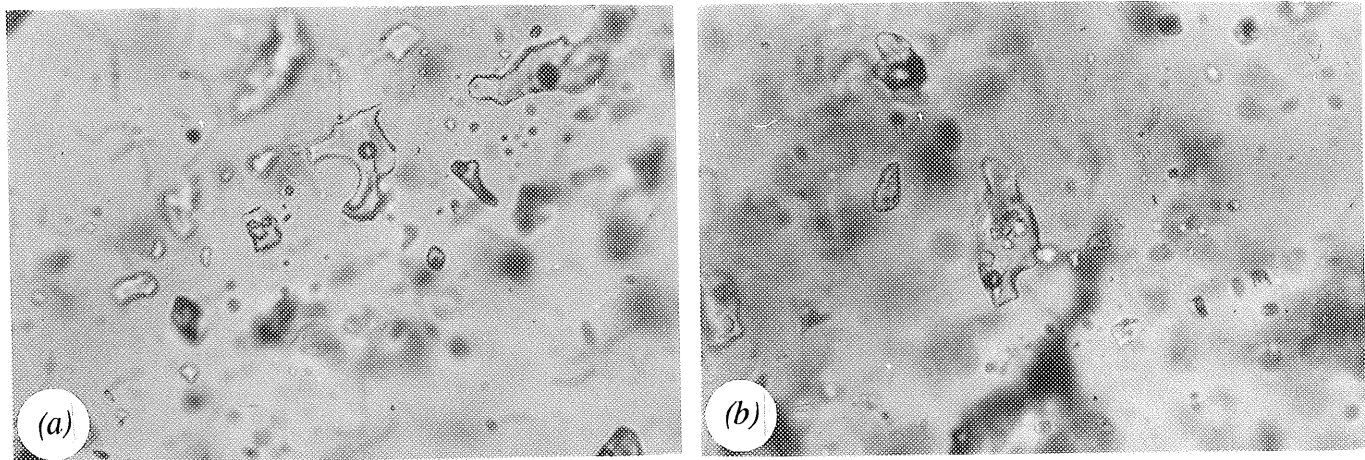


Figure 4: (a). Type 1 fluid inclusions in quartz at room temperature. These are filled with an aqueous liquid and a carbonic phase. (b). Type 2 inclusions typified by multiple daughter crystals. Late-stage Type 3 aqueous inclusions occur with or without vapour bubbles. See text for detailed discussion.

vapour ratio varies to such an extent that some inclusions appear as two phase inclusions, showing an aqueous liquid and carbonic vapour or a carbonic liquid and vapour bubble. Contemporaneity of aqueous and carbonic fluid inclusions in the late fractures is suggested by the occasional occurrence of aqueous and carbonic inclusions along the same healed fracture. The compositional continuum shown by these fluids strongly suggests a close genetic relationships, which, in turn, supports contemporaneity of these fluids. The morphology of these, the dominant inclusion type, varies from irregular to rounded, with equidimensional negative crystal shapes also developed. The size of the inclusions ranges from 5 to 30 μm .

Final melting temperatures (T_m) of the aqueous phase range from -21.2° to -4.3°C, corresponding to a salinity range of 23.5 to 5.5 wt% eNaCl. Most inclusions containing carbonic species decrepitate in the temperature range between 170° and 290°C, prior to bulk homogenization (T_h). This is a common feature for the majority of reefs and decrepitation at such relatively low temperatures suggests high internal fluid pressures. The T_h measurements obtained, occur in the range 105° to 255°C, corresponding to high bulk density of 0.857 to 1.053 g/cm³. Comparison of homogenization and final melting temperatures for the various reefs show different salinities for the different reefs and confirm the salinity ranges within individual reefs (Fig. 5).

First melting temperatures for the carbonic phase are slightly below the value for pure CO₂, and support the presence of other gaseous species, such as CH₄ and N₂. Two distinct populations of carbonic inclusions are recognised on the basis of the CO₂ homogenization temperatures, with histogram peaks occurring at 10° and 23°C respectively. The different densities, indicated by these different temperatures, suggest that these fluids represent different pulses of fluid influx. However, it was not possible to optically distinguish the different density fluid inclusions.

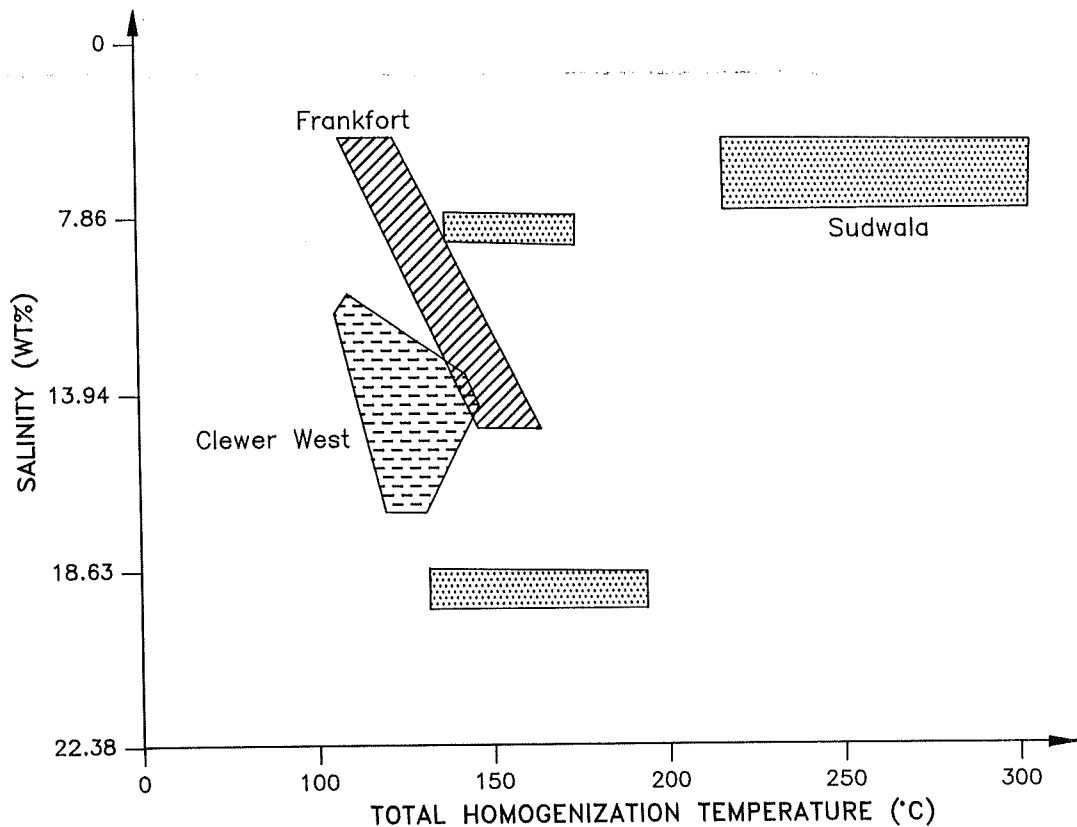


Figure 5: Homogenization temperature versus salinity for Type 1 inclusions. The boxes identify the domains of the mineralizing fluids of different deposits.

Type 2 inclusions

This type of inclusion is characterized by a minimum of three phases at room temperature, namely an aqueous liquid, a vapour bubble and at least one daughter crystal (Fig. 4b). Low first ice melting temperatures, plus the presence of a daughter crystal in addition to halite (or sylvite) indicates that additional fluid components are present (possibly calcium- or magnesium-chlorides). Carbonic species are frequently present, but are not visible and are only evident in the formation of clathrates that obscure accurate determination of final melting temperatures. This type of inclusion is common in the vertical reefs, but does not occur in the stratabound flat reefs. Homogenization temperatures of these inclusions range from 105° to 165°C while dissolution temperatures for the daughter phases plot in the range 220° to 245°C, corresponding to salinities of around 33 wt% eNaCl.

Type 3 inclusions

These inclusions contain an aqueous liquid, with or without a vapour bubble at room temperature (Fig. 4c), and are believed to be the latest-formed inclusion type. They are found in both the milky and clear quartz varieties. However, in the volumetrically minor

late-stage clear quartz the predominant inclusion type is a low salinity aqueous inclusions, while carbonic and aqueous saline inclusions are rare. Cross-cutting relationships between type 3 and type 1 inclusions prove that the former post-date the carbonic-rich inclusions. Final melting temperatures centred around -4.5°C (corresponding to a salinity of about 7 wt% eNaCl), and homogenization temperatures ranged from 110° to 135°C (density range 1.001 - 0.982 g/cm³). The absence of vapour bubbles in many of these late fluid inclusions suggest low entrapment temperatures, and confirms the late temporal relationship.

Quadrupole mass spectrometer gas analyses

Quadrupole mass spectrometer (QMS) gas analyses were performed on fluid inclusion plates less than 2 mm in diameter with a total mass of less than 50 mg. Gases were released from quartz wafers by crushing the samples at 110°C under vacuum in a modified Nupro[®] valve, from which they were passed directly into a VG SXP600 quadrupole mass spectrometer via a short conduit designed to maximize conductance and minimize adsorption between sample and ionizing filament. Inclusion fluids were released from native gold grains by heating small samples under vacuum in a Vycor[®] tube until the inclusions decrepitated (Fig. 6). Gases liberated in this manner passed directly into the quadrupole source and produced episodic signal bursts that probably represent individual inclusions. Gas species from individual inclusions with abundances of less than 0.50 mole% can not be reported with confidence and were therefore omitted. Data for 10 user-specified masses were collected in a cycling period of about 0.2 second, which permitted simultaneous determination of H₂O, CO₂, CH₄, C₂H₆, N₂, Ar, H₂S, SO₂, HCl and H₂. Total response for each mass was obtained by integrating under the individual response-time curve for each mass from the time of crushing until the signal returned to background levels. The integrated response for each mass was converted to mole fraction for the gases of interest using a matrix-inversion procedure that takes into account fragmentation patterns and relative sensitivities (to N₂) determined for the specific instrument (Jones and Kesler, 1992).

Results from bulk fluid inclusion gas analyses are presented in Table 1. Great care has been taken to ensure the dominance of Type I fluid inclusions within the pure quartz specimens. This was achieved through handpicking of doubly polished quartz chip fragments under microscopic examination. However, it is inevitable that these analyses of solute compositions are contaminated by other fluid populations (Roedder, 1990) and thus represents a partially time-integrated view of the fluid chemistry. H₂O is by far the most dominant volatile component in the Sabie-Pilgrim's Rest fluid inclusions and typically comprises 95-99 mole per cent of the inclusion fluid. CO₂ comprises most of the remaining volatile component and the other gases are generally present in amounts smaller than 1 mole per cent. CH₄/CO₂ ratios are consistent and significantly higher, compared to gas discharges from volcanic systems e.g. the Guanacaste Geothermal Province (Giggenbach and Soto, 1992), suggesting more reduced fluid conditions in the Sabie-Pilgrim's Rest Goldfield compared to volcanic or geothermal systems. In general, two groups of gases can be distinguished. The vertical reefs and the quartz reefs from lower down in the stratigraphy contain the highest concentrations of Ar and HCl, whereas the upper reefs contain larger CO₂ and CH₄ concentrations (Figs. 7 & 8). The higher abundances of carbonic species in the stratigraphically higher reef horizons indicate interaction of the hydrothermal fluid with the dolomitic host rocks, liberating carbonic gases. The scatter is likely to be due to the mixture

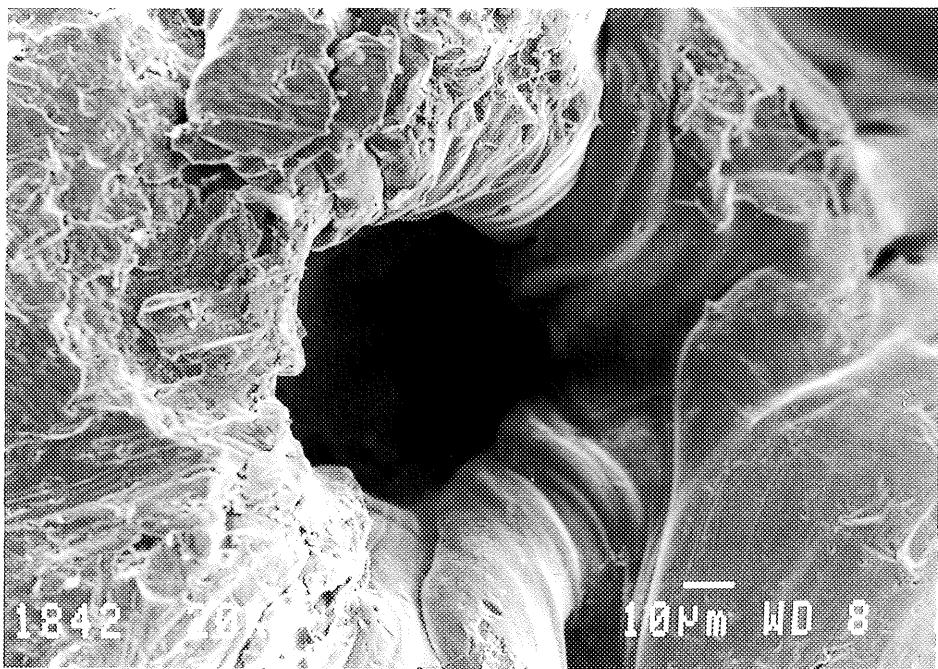


Figure 6: Cavity of a decrepitated fluid inclusion in a pure gold grain. Diameter of cavity $\approx 50 \mu\text{m}$.

of fluid populations, as analytical results were obtained from bulk extraction techniques. The $\text{H}_2\text{S}/\text{SO}_2$ ratio of the inclusion fluid is approximately 3, much higher than the equilibrium ratio for gases from geothermal systems (Giggenbach *et al.*, 1990). This appears to reflect the presence in the inclusions of SO_2 and possibly thiosulphate (Landis and Rye, 1989; Kesler *et al.*, 1991). However, the relative scarcity of H_2 in the inclusion fluid analyses might suggest that this SO_2 was produced by post-depositional leakage of H_2 out of the inclusions. Diffusion of H_2 out of an inclusion is accompanied by oxidation of H_2S to SO_2 . On the basis of relative N_2 , Ar and CO_2 contents (Fig. 8), large-scale fluid interaction with air-saturated meteoric water is ruled out. Average N_2/Ar ratios centre around 4.5 (maximum=19.6), which are well below those of air (84) or air-saturated ground water (38). In a plot of CO_2 - N_2 - Ar abundances (Fig. 8), most of the fluid inclusion analyses extend outward from the composition of gases in high temperature fumaroles of suspected magmatic origin (Giggenbach *et al.*, 1990), parallel to a mixing line towards the composition of air-saturated water. In general, analyses of porphyry and acid-sulphate deposits, in which magmatic gas contributions should be largest, plot closest to the fumarole compositions. Samples such as porphyry-related tin-tungsten veins, Mississippi Valley Type Pb-Zn and micron-gold deposits, all associated with sedimentary rocks (a possible source of N_2) plot above this line. The absence of air contamination from the Sabie-Pilgrim's Rest gas analyses is also indicated by the fact that most analyses plot below the mixing line between air and fumarole/magmatic compositions. High Ar contents in some samples probably result from the radiogenic decay of potassium, with subsequent incorporation into fluid inclusions.

H_2O and CO_2 concentrations, as determined from individual fluid inclusion release profiles (Table 2) from pure gold samples, show fairly homogeneous populations, with the exception of fluids released at higher temperatures, which typically contain more CO_2 . In

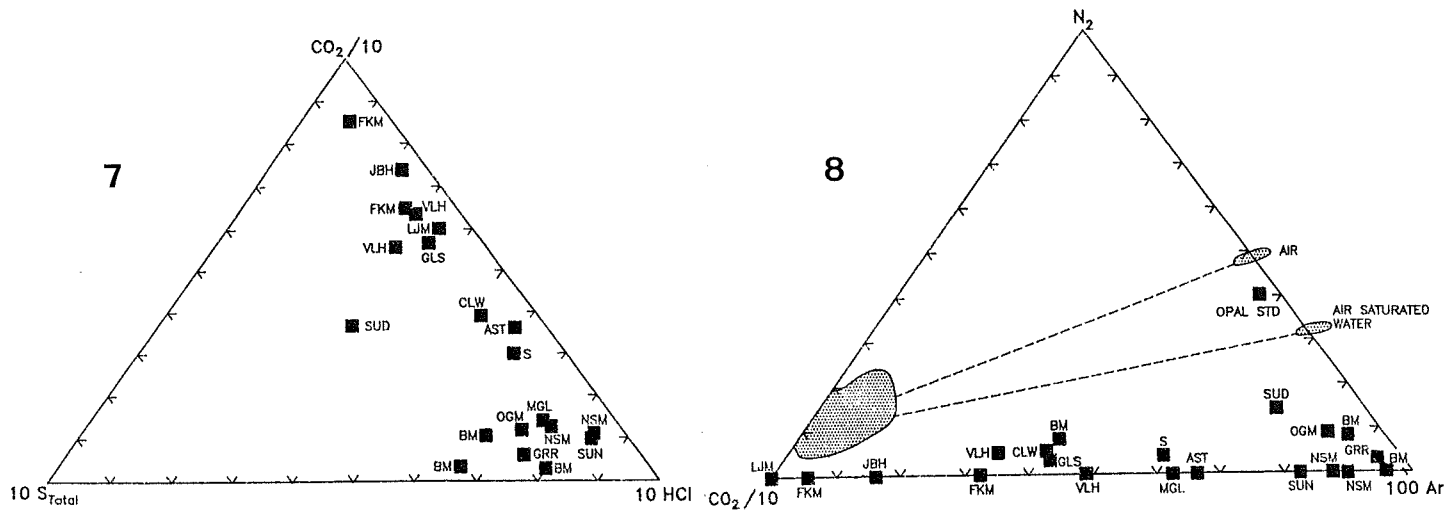


Figure 7: Relative CO_2 , S_{Total} and HCl contents of hydrothermal gases from quartz specimens of the Sabie-Pilgrim's Rest Goldfield.

Figure 8: Ternary diagram comparing the CO_2 , N_2 and Ar contents of inclusion fluids from the Sabie-Pilgrim's Rest Goldfield with those of volcanic fumaroles and air and air-saturated meteoric H_2O . The tie lines from air and water to CO_2 represent possible mixing lines between air and/or meteoric water with magmatic gas.

one instance H_2O and CO_2 were released abruptly, followed by a more gradual CO_2 release. This peculiar cracking pattern was interpreted as representative of a fluid inclusion containing a carbonate daughter crystal. The presence of such daughter crystals in quartz-hosted inclusions were confirmed by Raman spectroscopic studies (Boer, 1993). The average

Table 2: Quadropole mass spectrometer gas analyses of individual fluid inclusions contained in pure gold, presented in mole %

	H_2O	CO_2	CO_2/H_2O
Low T	98.15	1.85	0.019
	96.97	3.03	0.031
	98.50	1.50	0.015
	98.16	1.84	0.019
	98.54	1.46	0.015
	80.12	19.88	contained carbonate burnoff
	96.08	3.92	0.041
	96.17	3.83	0.040
High T			

$\text{CO}_2/\text{H}_2\text{O}$ ratios for the fluids from the gold (0.025) compare favourably with those from the quartz specimens (0.035), suggesting that the chemical composition of the ore-bearing fluid could not have been much different from those discussed above. The gas data presented are in agreement with a presumed magmatic-hydrothermal nature of the Sabie-Pilgrim's Rest system, but also suggest small contributions of carbonic fluids of possible sedimentary origin.

LIGHT STABLE ISOTOPE RELATIONSHIPS

Quartz oxygen isotope data

Oxygen extraction from silicates were performed in accordance with the technique of Borthwick and Harmon (1982) as well as using the laser-based technique of Sharp (1990). NBS-28 and NBS-30 were used as reference standards and yielded, respectively, values of 9.6 ‰ (9.5 ‰ for the laser-ablation technique) and 5.1 ‰ V-SMOW. The $\delta^{18}\text{O}$ -values of duplicated samples were generally within 0.2 ‰ about the mean. All oxygen isotope values are reported in δ -notation in per mil units relative to V-SMOW.

A total of 32 quartz samples from both the vertical and horizontal reefs as well as the sill/dyke associated reefs, covering a vertical span of approximately 350m, were analyzed, in duplicate, for their $\delta^{18}\text{O}$ values and the data is presented in Table 3. The vertical reefs yielded an average $\delta^{18}\text{O}$ value of 14.2 ‰ ($S_x=0.34$; $n=14$), a slightly higher average of $\delta^{18}\text{O}=16.1$ ‰ ($S_x=1.77$; $n=48$) was obtained for the various horizontal reefs, while the diabase sill/dyke associated deposits showed an average value of $\delta^{18}\text{O}=20.7$ ‰ ($S_x=1.23$; $n=6$). The data in Figure 9 demonstrate a progressive decrease in ^{18}O content with increasing depth. Variation in $\delta^{18}\text{O}$ values within individual quartz reef systems are restricted e.g. Frankfort Mine $\delta^{18}\text{O}=16.1$ ‰ ($S_x=1.2$; $n=8$). Fluid $\delta^{18}\text{O}$ values were calculated from quartz mineral values using the equation of Matsuhisa *et al.* (1979) in Table 3. These values ($\delta^{18}\text{O}_{\text{Fluid}}$) ranged from 8.7 to 9.5 ‰ for the vertical reefs, 6.2 to 13.8 ‰ for the flat reefs and 14.2 to 16.8 ‰ for the dyke/sill associated deposits, and overlap the range for magmatic waters (5.5 - 9.0 ‰ ; Taylor, 1979).

Variations in the $\delta^{18}\text{O}$ values of hydrothermal quartz occur in response to a number of independent parameters. Quantitatively, the most important of these are the $\delta^{18}\text{O}$ value of the fluid and the ambient temperature at which fluid-mineral isotopic equilibrium is attained (Kerrich, 1987). At the site of mineralization, the $\delta^{18}\text{O}$ of hydrothermal fluids may be modified by (1) exchange reactions with wall rocks; (2) precipitation or solution of an oxygen-bearing phase either depleted or enriched in ^{18}O with respect to the fluid, and in a closed system; (3) immiscible separation of CO_2 ; or (4) mixing with an isotopically distinct fluid reservoir. Options (1) and (2) may be ruled out based on arguments presented above for high fluid/rock ratios in the hydrothermal conduits. Moreover, the solubility of most hydrothermal minerals in the deposits are sufficiently low that their precipitation is accompanied by negligible isotopic shifts in the fluid phase. Fluid mixing can probably be eliminated as a first order effect, from the observation that the ore-forming solutions were close to or greater than lithostatic pressures during hydraulic fracture, fluid advection, and reef-forming events (Harley and Charlesworth, 1993), and from the consistency of paragenetic assemblages in successive reef stages. However, some mixing of deep pore water is indicated. Taking these factors into account, the uniformity in $\delta^{18}\text{O}$ values of quartz

Table 3. $\delta^{18}\text{O}$ and $\delta^{18}\text{O}_{\text{Fluid}}$ values for quartz from vertical and horizontal reefs as well as sill-associated gold mineralized localities. Values were determined using the conventional extraction method as described by Borthwick and Harmon (1982). While those values in parenthesis represent data generated following the laser-based extraction method of Sharp (1990). $\delta^{18}\text{O}_{\text{Fluid}}$ values were calculated from quartz mineral values using the equation of Matsuhisa *et al.*, (1979). All values are expressed in per mil notation relative to VSMOW. Abbreviations for the different localities are as follow: AST - Astra; BRH - Browns Hill; CLW - Clewer West; CLS - Clewer South; DRM - Desireé; FKM - Frankfort; GLS - Glynn's Lydenburg Sheba; GRR - Gregory; JBH - Jubilee; LJM - Little Joker; MAM - Mamre; MGL - Morgenzon; NSM - Nestor; OGM - Olifantsgeraamte; RFT - Rietfontein; SUD - Sudwala; SUN - Sunlight; THH - Theta Hill; VLH - Vaalhoek

Sample	$\delta^{18}\text{O}$	$\delta^{18}\text{O}_{\text{Fluid}}$	Sample	$\delta^{18}\text{O}$	$\delta^{18}\text{O}_{\text{Fluid}}$
Flat reefs			Vertical reefs		
FKM075A	16.3 (15.7)	10.7	RFT113	14.8	9.5
FKM075B	14.7 (14.2)	9.1	SUN003	14.2	8.9
FKM076A	17.4	12.1	GRR099	14.2	8.9
FKM076B	17.2	11.9	GRR106	14.1	8.8
FKM077A	17.2	11.9	GRR107	14.2	8.9
FKM077B	16.5	11.2	GRR108	14.3	9.0
LJM090	14.0 (13.9)	8.6	AST109	14.0	8.7
NSM093	14.4 (14.1)	8.9	Sill/dyke associated reefs		
BRH112	19.7	14.4	VLH040	22.1	16.8
MAM103	15.2	9.9	OGM082	19.5	14.2
MAM104	14.7	9.4	OGM083	20.1	14.8
CLH110	11.5	6.2			
CLH111	16.0	10.7			
BRH112	19.7	14.4			
MGL032	16.4	11.1			
MGL033	16.2	10.9			
CLS038	16.7	11.4			
JBH043	18.5	13.2			
DRM044	19.1	13.8			
GLS052	16.6	11.3			
CLW013	16.7	11.4			
CLW017	17.8 (17.8)	12.5			
THH030	15.4	10.1			

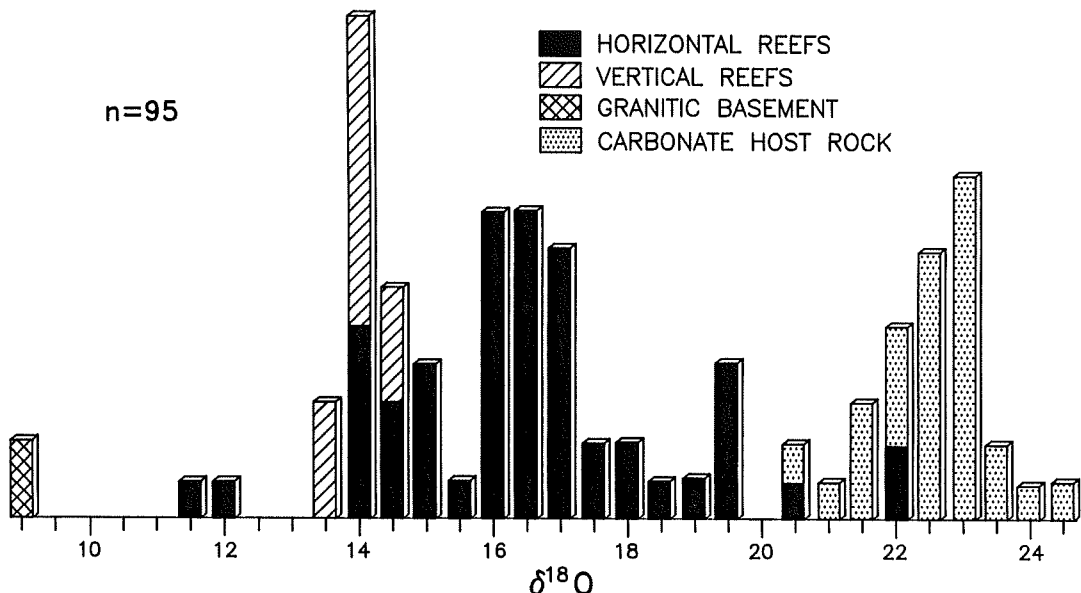


Figure 9: $\delta^{18}\text{O}$ values for quartz separates from various Au-bearing reefs in the Sabie-Pilgrim's Rest Goldfield.

in the individual Au-reef deposits, implies a corresponding homogeneity in both the $\delta^{18}\text{O}$ values of hydrothermal fluids, and a fairly consistent ambient temperature of mineralization. Furthermore, these $\delta^{18}\text{O}_{\text{Quartz}}$ relationships imply a fluid-dominated system along the hydrothermal conduits.

Pyrite sulphur isotope data

The sulphur in pyrite was converted to SO_2 using the Cu_2O oxidation method of Coleman and Moore (1978). Sixty pyrite samples from within the quartz reefs were analyzed for $\delta^{34}\text{S}$ which ranged from -2.8 ‰ to $+3.1\text{ ‰}$. $\delta^{34}\text{S}$ values for pyrite from the lower reef horizons fall into a restricted range close to 0 ‰ $\delta^{34}\text{S}$ and low variance, characteristic of magmatic sulphur. The upper reefs show a tendency toward negative $\delta^{34}\text{S}$ values. This tendency coincides with the changeover toward negative $\delta^{34}\text{S}$ numbers of the sulphides from the shales, as measured by Cameron (1982). Cameron (1982) identified an isotopic transition zone in the lower Malmani Subgroup, above which the sulphides from the shales were derived from reduction of sulphate, with both biogenic and inorganic processes being involved. The shift towards negative numbers in the reef-associated sulphides could be ascribed to limited isotopic exchange with the latter group of shale-hosted sulphides.

Fluid inclusion stable isotope data

Measurements of $\delta^{18}\text{O}$, δD and $\delta^{13}\text{C}$ were performed on fluids from decrepitated fluid inclusions in selected quartz samples, following the method described by Vennemann and O'Neil (1993). These data are presented in Table 4. The hydrogen isotopic composition of water in fluid inclusions extends from -37 to -67 ‰ . The magnitude of the observed dispersion cannot be accounted for by mixing of fluids from depleted and enriched δD fluid reservoirs. Any such mixing would be reflected in shifts of both δD and $\delta^{18}\text{O}$ fluid, but the uniformity of $\delta^{18}\text{O}$ fluid values (as measured and calculated from quartz data) eliminates this possibility (Fyon *et al.*, 1983). Rather, the observed range in $\delta\text{D}_{\text{H}_2\text{O}}$ may be due to the

Table 4. Light stable isotope values (δD , $\delta^{13}C$ and $\delta^{18}O$) of extracted inclusion fluids from flat reefs (Clewer West - CLW), vertical reefs (Gregory - GRR & Rietfontein - RFT) and sill associated reefs (Olifantsgeraamte - OGM). Data are presented relative to per mil VSMOW

Sample	δD_{H_2O}	$\delta^{13}C_{CH_4}$	$\delta^{13}C_{CO_2}$	$\delta^{13}C_{Total}$	$\delta^{18}O_{Total}$
OGM082	-47.0	n.d.	-11.7	-11.7	n.d.
GRR107	-37.3	n.d.	-2.3	-2.3	n.d.
CLW017	-53.3	n.d.	-10.8	-10.8	n.d.
RFT001	-67.6	-36.0	-3.6	-4.8	6.5
CLW017	-53.5	-30.8	-0.3	-1.4	15.4

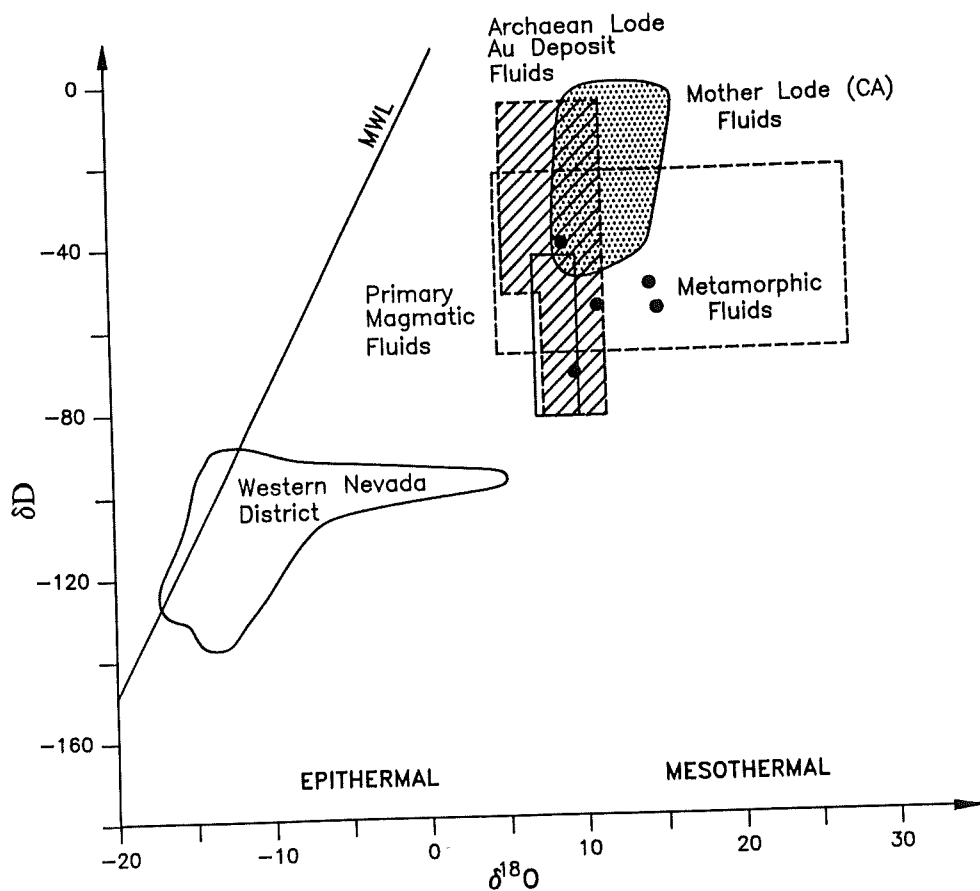


Figure 10: A δD vs $\delta^{18}O$ plot depicting the stable isotope geochemistry of Sabie-Pilgrim's Rest ore-bearing fluids. MWL - Meteoric Water Line. Note that the stable isotope chemistry of the ore-bearing fluids requires that the deposits formed from a predominantly magmatic fluid.

presence of H_2 and/or CH_4 in the aqueous fluid, as confirmed by the gas chemistry data (Table 1). When plotted on a $\delta^{18}O$ vs δD diagram (Fig. 10), the Sabie-Pilgrim's Rest data coincide with the primary magmatic water field, and show no signs of major isotopic interaction with meteoric or basinal water. The Sabie-Pilgrim's Rest δD and $\delta^{18}O$ data are distinctly different from epithermal, volcanic associated massive sulphide and Mississippi Valley Type deposits (e.g. Ohmoto, 1986), and show a correspondence to the stable isotopic values from the precious metal veins from Archaean Au deposits such as Macassa, McIntyre-Hollinger and Kerr-Addison (Bursnall, 1989). Although it is not possible to discriminate between primary hydrothermal reservoirs using hydrogen and oxygen data alone, the correspondence of the Sabie-Pilgrim's Rest data with Au vein deposits with known magmatic fluid contributions, suggests a predominant magmatic component in these hydrothermal fluids.

^{13}C isotope values for fluid inclusions fall within the range -11.7 to -1.4 per mil, whereas the average $\delta^{13}C$ value for carbonate minerals from reefs are -2.4 per mil (Schidlowski *et al.*, 1975). These data suggest that hydrothermal fluids may have acquired carbonate (CO_2 , H_2CO_3 , HCO_3^-) from carbonate rocks through dissolution or thermal decarbonatization. Given the physico-chemical conditions during entrapment of these inclusion fluids, as discussed below, then $\delta^{13}C_{Ca,Mg(CO_3)_2} \approx \delta^{13}C_{Fluid}$ (Ohmoto and Rye, 1979). At 300°C the fractionations between oxidized carbon species (CO_3^{2-} , H_2CO_3 , HCO_3^-) in solution are small (Bottinga, 1969). The calcite- HCO_3^- fractionation is $\sim +1\text{‰}$ at 300°C, such that calcite of -3‰ would have been precipitated from a fluid where $\delta^{13}C_{HCO_3^-} \approx -4\text{‰}$ (Kyser, 1987). This can account for the Rietfontein, Gregory and some of the Clewer West values (Table 4), but does not explain the large shifts in the Olifantsgeraamte and some Clewer West samples. Interaction of the hydrothermal fluid with graphite can generate methane following the reaction, $C + 2H_2O \rightleftharpoons CH_4 + 2[O]$, where $[O]$ represents oxygen bound in CO_2 and/or carbonate. Methane is depleted relative to CO_2 by 24‰ at 300°C. Accordingly, the $\delta^{13}C$ of hydrothermal CO_2 could be buffered to -11‰ (at 300°C) by equilibrium exchange with graphite of -27‰ (Bottinga, 1969). Such an isotopic equilibrium between CO_2 and CH_4 is possible without obtaining chemical equilibrium (Giggenbach, 1982). It is clear that the source, or sources, of carbon cannot as yet be resolved with certainty. However, neither magmatic nor meteoric sources alone can account for the observed distribution of $\delta^{13}C$ values.

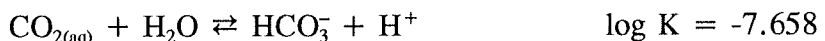
DISCUSSION

Temperature, pressure and fluid composition

The confining pressure of the Sabie-Pilgrim's Rest-type mineralization is not well constrained due to the lack of suitable geobarometers. The observed fluid inclusion relationships within the Type 1 fluids is consistent with a low degree of unmixing, or phase separation. Fluid unmixing may occur in response to fluid-pressure fluctuations. These changes in turn, may be related to brecciation and resealing of the quartz reefs and are consistent with the emplacement mechanism and deformational history of these quartz reefs (Harley and Charlesworth, 1993).

Dissolution of daughter crystals after vapour homogenization indicates relatively high entrapment pressures, taking into account the precautions stipulated by Roedder and Bodnar (1980). A reconstruction of the overburden at the time of quartz reef mineralisation indicates a thickness of approximately 7 to 8 km (Button, 1986) which corresponds to a lithostatic pressure of 2.2 to 2.5 kb (1 kb/3.2 km). This pressure estimate corresponds to a temperature of about 320°C, using the Jacobs and Kerrick (1981) and Holloway (1981) equations of state to calculate isochores for the above fluid characteristics. This temperature estimate is confirmed by the arsenopyrite thermometer (Kretschmar and Scott, 1976) which yielded a value of 320°C (Boer, 1993; Harley, 1993).

Chemical characteristics of the Sabie-Pilgrim's Rest ore fluids may be estimated using mineral stabilities and fluid inclusion gas data. A pH estimate can be calculated using the white mica composition and assuming solid solution between stoichiometric paragonite and muscovite. The micas are spatially and paragenetically related to late-stage, fracture-hosted gold grains, which are developed within coarse-grained pyrite (Harley and Charlesworth, 1991). Thermodynamic activity calculations of end-member components using homologous site mixing models (Aagaard and Helgeson, 1983) give consistent activities for stoichiometric paragonite and muscovite (*a*paragonite = 0.002; *a*muscovite = 0.686 ± 0.077) (Harley, 1993; Boer and Harley, *in press*). The composition of muscovite (*sensu lato*) constrains the Na/K ratio of the equilibrium fluid from which such micas crystallized (Helgeson and Aagaard, 1985). The fluid in equilibrium with the muscovites from the Transvaal Sequence quartz reef deposits, and by inference, the gold (given the known relative timing of gold and muscovite within the reef) is indicated to have a Na:K ratio of 0.1 (Harley, 1993; Boer and Harley, *in press*). A moderately acidic pH estimate of 4.2 is obtained at 320°C and 2.2 kb for the muscovite/K-feldspar stability boundary, with neutral pH value under these conditions being 5.1. By using the reaction;



(Calculated using SUPCRT92; Johnson *et al.*, 1992)

the authors were able to calculate a pH range of 3.7 to 4.2 for the Sabie-Pilgrim's Rest fluids, for an average CO₂ concentration of 1.83 molal ($\gamma_{\text{CO}_2} = 2.26$ (calculated from Patterson *et al.*, 1981); $a\text{CO}_2 = 4.13$) as obtained from gas data (Table 1). This is consistent with the muscovite stability and $a\text{K}^+ < 10^{-1}$.

The oxidation state of the fluids can be estimated in several ways. The common sulphide assemblage pyrite + chalcopyrite + arsenopyrite found in many of the Sabie-Pilgrim's Rest district deposits implies that the sulphur species in the fluid are not highly oxidized. As shown in Figure 11, the reduced species H₂S is the dominant sulphur species in the fluid, given such a mineral assemblage. Thus, the range of $\delta^{34}\text{S}$ of -2.8 to 3.15 ‰ for the Sabie-Pilgrim's Rest reef pyrite, should reflect the $\delta^{34}\text{S}$ range of the reef fluid (as discussed by Ohmoto and Rye, 1979). With this $\delta^{34}\text{S}$ range for the fluid, the sulphur may have been derived from interactions with metavolcanic rocks at depth, which is unlikely in the Sabie-Pilgrim's Rest Goldfield, and/or from magmatic sources (Ohmoto and Rye, 1979; Ohmoto, 1986).

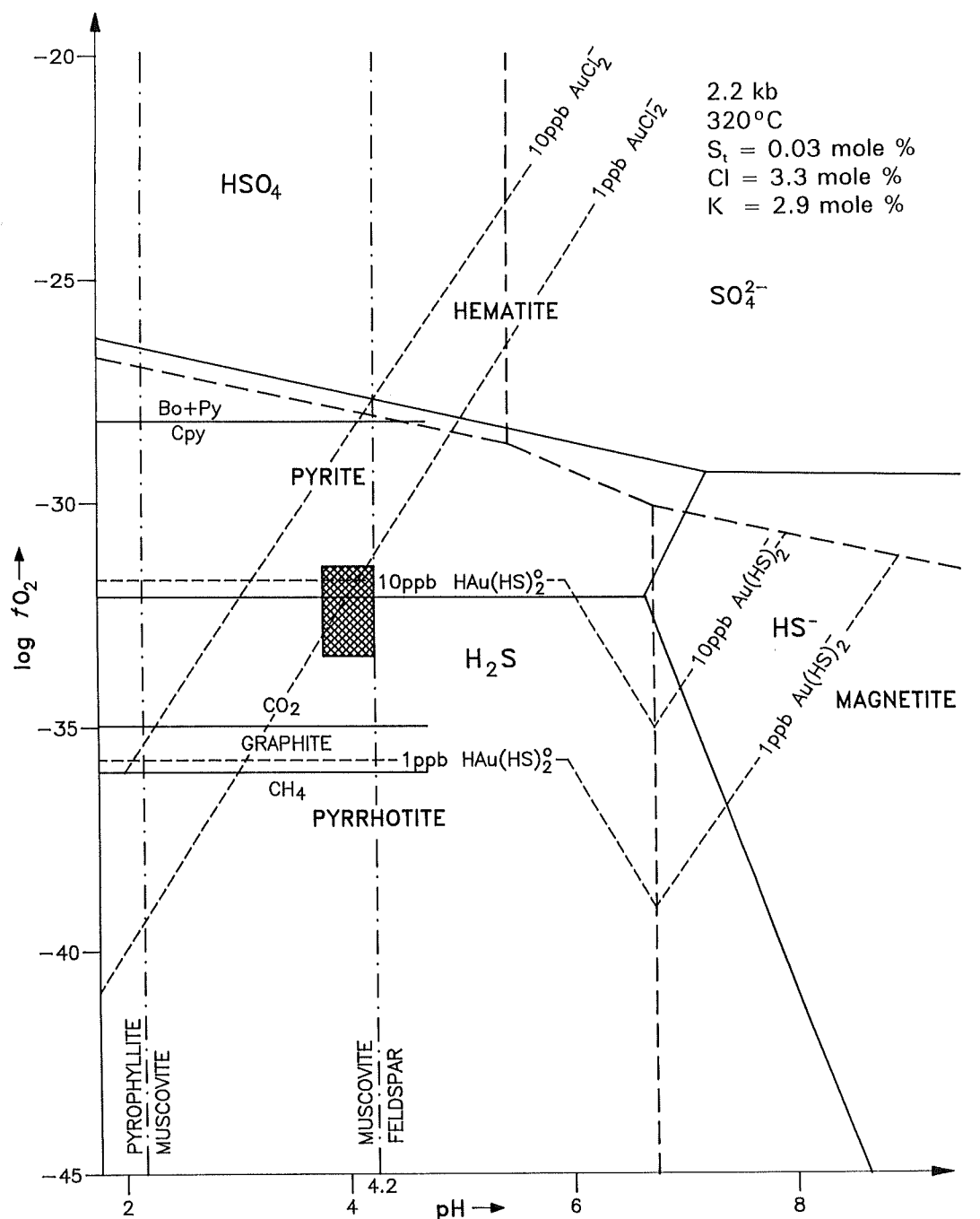
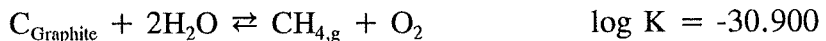


Figure 11: Composite $\log f\text{O}_2$ vs pH diagram for Sabie-Pilgrim's Rest conditions. Calculated using SUPCRT92; Johnson *et al.* (1992). Shaded area represents an approximation of activities of reef forming fluids, based on average gas analytical results.

The stability field of graphite, ubiquitously developed along reef margins, was calculated (using SUPCRT92; Johnson *et al.*, 1992), using the pure species equilibrium;



and,



From bulk gas analysis data (Table 1) it is found that the ore fluids, in some instances, straddle the CO_2 -graphite boundary, with the $\log aCO_2$ ranging between 0.034 and -0.201 (Fig. 10). As discussed by Holloway (1984), fluid compositions coexisting with graphite at $T < 400^\circ\text{C}$ are essentially two binary systems: $CO_2\text{-H}_2O$ and $CH_4\text{-H}_2O$. However, the low abundance of carbonic species in the Sabie-Pilgrim's Rest fluids suggests that the latter fluids mixed to form a single, homogeneous, supercritical fluid (Holloway, 1984). The range in $\delta^{13}\text{C}$ values for the Sabie-Pilgrim's Rest Goldfield carbonates, is consistent with the presence of small amounts of CH_4 in the fluids, due to the large $\Delta_{\text{CH}_4\text{-CO}_2}$ fractionation factor (Bottinga, 1969).

Gold solubility and depositional mechanisms

The results of this study enable the authors to summarize the following characteristics of the mineralizing fluids which formed the Sabie-Pilgrim's Rest deposits: A temperature of approximately 320° and a pressure range of 2.2 to 2.5 kb is suggested. The $X_{\text{Carbonic species}}$ in the fluids is about 0.05 as determined by the QMS gas analyses. The fluid salinities are intermediate, ranging from 5.5 to 23.5 wt% eNaCl (average salinity ≈ 10 wt% eNaCl) as indicated by $T_{m,ice}$ measurements. The pH was slightly acidic at 3.7 to 4.2. The fO_2 was around $10^{-32.5}$ and the fH_2S_g was between 3 and 10 bars (calculated from X_{H_2S} in the QMS data), which corresponds to aH_2S_{aq} of between $10^{-2.5}$ to $10^{-2.8}$.

Using these fluid characteristics, speculation on the gold speciation and precipitation mechanism is possible. Experimental data on the Au bisulphide complexes (Hayashi and Ohmoto, 1991; Shenberger and Barnes, 1989; Seward, 1973) for the conditions outlined above indicate solubilities between 1 and 10 ppb. Solubility calculations of Au as chloride complexes, using the data of Henley (1973) yields solubilities that are an order of magnitude less than the Au bisulphide complexes (Fig. 11). Precipitation mechanisms pertinent to a fluid transporting gold as a bisulphide complex include: a decrease in T at constant pH; oxidation of the complex; pH reduction; and reduction in sulphur activity in the fluid by sulphide precipitation. Several of these possibilities are exemplified in the reaction $Au_s + 2H_2S_{aq} \rightleftharpoons Au(HS)_2^- + \frac{1}{2}H_{2,g} + H^+$ (Hayashi and Ohmoto, 1991). Given the association of gold with various sulphides noted at many mines in the Sabie-Pilgrim's Rest Goldfield (Harley and Charlesworth, 1992; Meyer *et al.*, 1986), the role of sulphide precipitation may be critical to gold precipitation. Variations in CO_2/CH_4 ratios noted in fluid inclusions from the Pamour Mine in the Timmins district in Canada, have been suggested as direct evidence of the influence of changing oxidation states on gold precipitation (Walsh *et al.*, 1988). However, the authors have no similar evidence from the QMS gas analyses for the Sabie-Pilgrim's Rest deposits. Furthermore, there is also no direct evidence that Au is transported as a bisulphide complex, although the calculated solubility of Au bisulphide complexes is an

order of magnitude higher compared to that of Au chloride complexes. Textural evidence pertinent to sulphide gold relationships (e.g. Harley and Charlesworth, 1992) indicates that gold could possibly have been precipitated onto sulphide surfaces by adsorption and subsequent reduction processes (Knipe *et al.*, 1992; Schoonen *et al.*, 1992; Bancroft and Hyland, 1990). Furthermore, Knipe *et al.* (1992) noted that the adsorption of Au is spatially related to arsenic-depleted micro-zones within pyrite. The fact that arsenic zonation is common within the Sabie-Pilgrim's Rest pyrite (Boer, 1993; Harley, 1993), makes this mechanism of gold precipitation feasible.

A GENETIC MODEL FOR THE SABIE-PILGRIM'S REST GOLDFIELD

Characteristic geological and geochemical features of the Sabie-Pilgrim's Rest Goldfield are similar to those displayed within the spectrum of mesothermal gold deposits. The observed characteristics contrast with those of epithermal gold deposits where temperatures of formation are similar, but inferred pressures of formation and $\delta^{18}\text{O}$ values are lower (Heald *et al.*, 1987), and the environment of ore deposition is markedly different. The Sabie-Pilgrim's Rest deposits are comparable in terms of mineralogy and physico-chemical conditions of mineralisation to the deposits of the Mother Lode of California (Weir and Kerrick, 1987), Archaean lode gold deposits (Kerrick, 1987), and gold deposits of the Canadian Cordillera (Goldfarb *et al.*, 1988). The recognised ore shoot structure is highly characteristic of mesothermal gold deposits (Colvine *et al.*, 1984; Peters, 1993). Studies by Cairnes (1937) and Walton (1987) showed that these structures are the result of brittle deformation following the main stage of vein formation and the subsequent influx of late-stage, gold-bearing fluids. High Au/Ag ratios, a general lack of isotopic and elemental zoning within the reefs, fluid inclusion petrographic properties, a temperature of formation around 320°C, a pressure of reef formation in the 2.2 to 2.5 kb range, amongst other factors, confirm the mesothermal nature the Sabie-Pilgrim's Rest Goldfield.

Evidence for widespread meteoric convection within the dolomites and shales of the Sabie-Pilgrim's Rest Goldfield is lacking. Stable isotope data clearly indicate that meteoric water was not a significant component within the ore fluids of the Goldfield. The consistent $\delta^{18}\text{O}$ values of the mineralizing fluids are also typical of those found in mesothermal systems of Archaean and Phanerozoic age, and contrast sharply with the relatively inhomogeneous data for epithermal gold systems (Kyser and Kerrich, 1990; Field and Fifarek, 1985). In part this represents a more uniform temperature of mineralization for mesothermal veins (Kerrick, 1987), as corroborated by microthermometric data presented above. In addition, the consistent data support a high fluid/rock ratio at the site of vein precipitation, so that the mesothermal vein-forming fluids are not appreciably modified by exchange with wall rocks. However, fluid inclusion gas analyses suggest limited contributions of carbonic fluid species to the hydrothermal fluid, probably due to dissolution of dolomitic wall rock. The uniformity of the stable isotopic values, the consistent CO_2/CH_4 ratios and fluid inclusion petrography, amongst other data, offers scant support for any model based on fluid mixing as the dominant mechanism for gold deposition in the Sabie-Pilgrim's Rest Goldfield (e.g. Anderson *et al.*, 1992).

Instead, the authors propose a hypothesis involving a saline fluid exsolving from a deep-seated granitic melt during crystallisation, probably associated with the granitic phase

of the Bushveld Complex. Experimental work by Bodnar (1992) has described high salinity fluids which exsolve from silicic magmas during the early stages of crystallization at 2 kb pressure. It is suggested that the high salinity fluid inclusions trapped within the vertical reef environment are representatives of a fluid of this nature. Vertically oriented structures represent suitable pathways to tap and focus the high-pressure fluids released at depth.

Restricted mixing with cooler pore fluids in the wall rocks and fluid-mineral reactions involving host lithologies are supported by inclusion gas and stable isotope chemistries. As reported above, most H_2O - CO_2 inclusions (Type 1) have variable CO_2 contents along individual fractures. This variation of the CO_2 content can be explained either by mixed entrapment of aqueous and CO_2 -rich fluids or by fluid unmixing during healing of the fracture. However, in a few samples there are healed fractures containing H_2O - CO_2 inclusions with constant phase ratios. The fact that in different samples these inclusions all contain approximately the same amount of CO_2 (Table 1), precludes the possibility that they might represent mixed entrapment of two immiscible fluids and suggests instead that these fluid inclusions might represent the parent homogeneous fluid from which the aqueous and CO_2 -rich fluids were locally derived. The presence of such inclusions also indicates that, at least for short periods of time during the fracturing of the reef minerals, the P-T conditions were such that the fluid was above the two-phase region and that the parent homogeneous fluid was trapped. Experimental data and thermodynamic calculations on the system H_2O - CO_2 - $NaCl$ indicate that the addition of $NaCl$ to the system extends the two-phase field to higher temperatures (Bowers and Helgeson, 1983). The coexistence of a moderately saline aqueous fluid containing small amounts of CO_2 with a very low salinity CO_2 -rich fluid containing small amounts of H_2O in the reefs, can thus be explained by unmixing (immiscibility) of a low salinity H_2O - CO_2 fluid. Bowers and Helgeson (1983) have shown that a high salinity H_2O -rich fluid can be produced by unmixing of a relatively low salinity H_2O - CO_2 fluid, because all the salt will fractionate into the H_2O -rich liquid phase rather than in the CO_2 -rich vapour phase. It is important to realize that such unmixing can be produced by progressive cooling of the fluid or by a pressure decrease. Other mechanisms can account for the variable proportions of CO_2 within type 1 inclusions. Reaction with wall rocks can explain the occurrence of some inclusions which have both high carbonic species contents as well as slightly higher salinities than other type 1 inclusions.

The exact source of gold remains uncertain. It is probable that the bulk of the gold was derived from the same magmatic source as the fluids. The limited amount of interaction with the host rocks seems to preclude leaching of gold from the fluid pathway as a dominant source of gold. Under the relatively low fO_2 conditions characterizing the Sabie-Pilgrim's Rest ore fluids, gold transport is calculated to have been almost exclusively by reduced sulphur complexes. Hence a source of aqueous sulphur was important to the transport of gold. Sulphur isotope ratios of sulphide minerals deviate from the inferred host rock values to such an extent that sulphur introduced from a distal source is necessarily indicated. This supports the suggestion that gold was derived mainly from a magmatic, rather than a remobilised sedimentary source.

The precipitation mechanisms that account for gold deposition within the Sabie-Pilgrim's Rest Goldfield deposits are elusive. In some deposits gold occurs primarily as fracture fills within sulphides (e.g. Elandshoogte, Clewer West, Malieveld) whilst in other

deposits gold is predominantly present as round inclusions within sulphides (Olifantsgeraamte, Vaalhoek). In some deposits both situations are common (e.g. Frankfort, Nestor) whereas in other deposits gold occurs mainly as free grains within quartz (e.g. Morgenzon). It is clear from the variations in mode of occurrence of gold within the various reefs that several mechanisms of precipitation were active and may have become locally dominant in some cases. Gold in quartz is probably best explained as a result of fluid immiscibility arising from pressure variations accompanying fracturing. Gold inclusions within sulphides may be a result of adsorption/reduction during sulphide growth (Knipe et al., 1992) or may be a result of decreasing aH_2S_{aq} accompanying sulphide precipitation (Neall, 1987). Gold in fractured sulphides similarly may be a consequence of changes in fluid chemistry as a result of fluid unmixing or a consequence of adsorption/reduction reactions, or both. All of these processes may have been active within any one reef unit. Prediction of the siting of gold with respect to the reef components is therefore not possible at the scale of the Goldfield and no single mechanism of gold precipitation can be given preference. Similarly, in other mesothermal deposits differences in gold siting and depositional control are equally unclear as a consequence of multiple mechanisms of deposition.

CONCLUSIONS

This study of the Sabie-Pilgrim's Rest Goldfield has indicated the following:

1. the lower age limit of gold mineralization is concurrent with the emplacement age of the mafic phase of the Bushveld Complex. Ore-bearing fluids show a predominantly magmatic character and were probably derived from a deep-seated portion of the granitic phase of the Bushveld Complex;
2. mineralization occurred at temperatures around 320°C, at pressures in the range 2.2 to 2.5 kb and at depths of 7 to 8 km;
3. oxygen isotope values of quartz from the vertical reefs yielded an average $\delta^{18}O$ value of 14.2 ‰. An average $\delta^{18}O$ value of 16.1 ‰ was obtained for the flat reefs, while the sill/dyke associated deposits showed an average $\delta^{18}O$ value of 20.7 ‰. ^{18}O content progressively decreases with increasing depth and $\delta^{18}O$ values in individual reef systems are remarkably homogeneous. $\delta^{34}S$ values of reef pyrite range from -2.8 to +3.1 ‰. δD , $\delta^{18}O$ and $\delta^{13}C$ values from inclusion fluids ($\delta D = -37$ to -67 ‰; $\delta^{18}O = +6.5$ to +15.4 ‰; $\delta^{13}C = -11.7$ to -1.4 ‰) coincide predominantly with values of primary magmatic water. Interaction of the ore fluid with the host rocks was of limited extent such that the magmatic isotopic, and gas chemistry signature of the fluids remains clear.
4. the pH of the ore-bearing solutions ranged from 3.7 to 4.2, oxygen fugacities were in the order of $10^{-32.5}$, and the activity of the H_2S species was between $10^{-2.5}$ and $10^{-2.8}$ with salinities ranging between 5.5 and 23.5 wt% eNaCl for the flat reefs and ≈ 30 wt% eNaCl for the vertical reefs;
5. the nature of the ore-bearing fluid was predominantly aqueous with < 5 mole % carbonic species, sulphur species and nitrogen. CH_4 and HC_1 concentrations were relatively high;

6. gold was probably transported as a bisulphide complex. Precipitation mechanisms for gold appear to be variable within any one deposit. Locally, a single mechanism may be dominant, in other cases several mechanisms are suggested to overlap in time and space; and
7. interaction of the ore fluid with the host rocks was of limited extent such that the magmatic isotopic and gas chemistry signature of the fluids is still clear. This limited interaction places constraints on the possible sources of gold. A magmatic, rather than a remobilised sedimentary source is favoured.

ACKNOWLEDGEMENTS

The authors thank Rand Mines (Mining & Services) Ltd and particularly Phil Bentley for permission to undertake this research and for assistance in the field and underground. Conventional whole rock oxygen isotope analyses were performed at the Department of Geological Sciences, University of Cape Town; sulphur isotopes were analyzed at the Schonland Research Centre for Nuclear Sciences, University of the Witwatersrand; radiogenic isotope analyses were completed at the Bernard Price Institute for Geophysical Research, University of the Witwatersrand; and laser-based oxygen isotope analyses, as well as light stable isotope and gas analyses of the inclusion fluids were performed at the Department of Geological Sciences, University of Michigan. Many discussions with Michael Harley and Phil Bentley are gratefully acknowledged. This work was partially sponsored by the National Geosciences Programme of the South African Foundation for Research Development and formed part of RHB's PhD project.

REFERENCES

- Aagaard, P. and Helgeson, H.C., 1983. Activity/composition relations among silicates and aqueous solutions: II. Chemical and thermodynamic consequences of ideal mixing of atoms on homologous sites in montmorillonites, illites and mixed-layer clays. *Clays and Clay Minerals*, v. 31, p. 207-217.
- Anderson, M.R., Rankin, A.H., and Spiro, B., 1992. Fluid mixing in the generation of mesothermal gold mineralisation in the Transvaal Sequence, Transvaal, South Africa. *European Jour. Mineral.*, v. 4, p. 933-948.
- Bancroft, G.M., and Hyland, M.M., 1990. Spectroscopic studies of adsorption/reduction reactions of aqueous metal complexes on sulphides surfaces. *Rev. Mineralogy*, v. 23, p. 511-558.

Beukes, N.J., 1973. Precambrian iron-formations of southern Africa: Econ. Geol., v. 68, p. 960-1004.

Bodnar, R.J., 1992. Can we recognize magmatic fluid inclusions in fossil systems based on room-temperature phase relations and microthermometric behaviour? Rept. Geol. Surv. Japan, v. 279, p. 26-30.

Boer, R.H. Physico-chemical conditions of mineralization in the Sabie-Pilgrim's Rest Goldfield, eastern Transvaal. Unpub. Ph.D thesis, Univ. of the Witwatersrand, Johannesburg (in prep).

Boer, R.H., and Harley, M., (1993). "Fluid mixing and the generation of mesothermal gold mineralisation in the Transvaal Sequence, Transvaal, South Africa" - A Discussion. European Journal of Mineralogy, (in press).

Bottinga, Y., 1969. Calculated fractionation factors for carbon and hydrogen isotope exchange in the system calcite-carbon dioxide-graphite-methane-hydrogen-water vapor. Geochim. Cosmochim. Acta, v. 33, p. 49-64.

Borthwick, J., and Harmon, R.S., 1982. A note regarding ClF_3 as an alternative to BrF_5 for oxygen isotope analysis. Geochim. Cosmochim. Acta, v. 46, p. 1665-1668.

Bowers, T.S., and Helgeson, H.C., 1983. Calculations of the thermodynamic and geochemical consequences of nonideal mixing in the system $\text{H}_2\text{O}-\text{CO}_2-\text{NaCl}$ on phase relations in geologic systems: Equation of state for $\text{H}_2\text{O}-\text{CO}_2-\text{NaCl}$ fluids at high pressures and temperatures. Geochim. Cosmochim. Acta, v. 47, p. 1247-1275.

Burger, A.J., and Coertze, F.J., 1975. Age determinations - April 1972 to March, 1974. Ann. Geol. Surv. S. Afr., v. 10, p. 135-141.

Bursnall, J.T., (Ed.), 1989. Mineralization in Shear Zones. Geol. Assoc. Canada Short Course Notes 6, 299 pp.

Button, A., 1973. A regional study of the stratigraphy and development of the Transvaal Basin in the eastern and northeastern Transvaal. Unpubl. PhD thesis, Univ. Witwatersrand, Johannesburg, 282 pp.

Button, A., 1986. The Transvaal sub-basin of the Transvaal Sequence. In: Anhaeusser, C.R. and Maske, S. (Eds.), Mineral Deposits of Southern Africa, Geol. Soc. S. Afr., p. 811-817.

Cairnes, C.E., 1937. Geology and mineral deposits of the Bridge River mining camp, British Columbia. Canada Geol. Survey Mem., v. 213, 140 pp.

Cameron, E.M., 1982. Sulphate and sulphate reduction in early Precambrian oceans. Nature, v. 296, p. 145-148.

Cathles, L.M., 1991. The importance of vein selvaging in controlling the intensity and character of subsurface alteration in hydrothermal systems: Econ. Geol., v. 86, p. 466-471.

Clendenin, C.W., Jr., 1989. Tectonic influence on the evolution of the early Proterozoic Transvaal Sea, Southern Africa. Unpub. Ph.D thesis, Univ. Witwatersrand, Johannesburg, 347 pp.

Coertze, F.J., Burger, A.J., Walraven, F., Marlow, A.G., and MacCaskie, D.R., 1978. Field relations and age determinations in the Bushveld Complex. Trans. Geol. Soc. S. Afr., v. 81, p. 1-11.

Coleman, M.L., and Moore, M.P., 1978. Direct reduction of sulphates to sulphur dioxide for isotopic analysis. Anal. Chem., v. 50, p. 1594-1595.

Colvine, A.C., Andrews, A.J., Cherry, M.E., Durocher, M.E., Fyon, A.J., Lavigne, M.J., Jr., Macdonald, A.J., Marmont, S., Poulsen, K.H., Springer, J.S., and Troop, D.G., 1984. An integrated model for the origin of Archean lode gold deposits. Ontario Geol. Survey Open-File Rept., v. 5524, 98 pp.

Crampton, D., 1974. A note on the age of the Matsap Formation in the northern Cape Province. *Trans. Geol. Soc. S. Afr.*, v. 77, p. 71-72.

Dowling, K., and Morrison, G., 1989. Application of quartz textures to the classification of gold deposits using North Queensland examples. *In: Keays, R.R., et al., (Eds.), The Geology of Gold Deposits: The Perspective in 1988: Econ. Geol. Mon.*, v. 6, p. 342-355.

Eriksson, K.A., Truswell, J.F., and Button, A., 1976. Palaeoenvironmental and geochemical models from an early Proterozoic carbonate succession in South Africa. *In: Walter, M.R., (Ed.), Stromatolites*, Elsevier, Amsterdam, p. 635-643.

Field, C.W., and Fifarek, R.H., 1985. Light stable-isotope systematics in the epithermal environment. *Rev. Econ. Geol.* 2, p. 99-128.

Fyon, J.A., Crocket, J.H., and Schwarcz, H.P., 1983. Applications of stable isotope studies to gold metallogeny in the Timmins-Porcupine camp. *Ontario Geological Survey Open File Report 5464*, 182 pp.

Giggenbach, W.F., 1982. Carbon-13 exchange between CO_2 and CH_4 under geothermal conditions. *Geochim. Cosmochim. Acta*, v. 46, p. 159-165.

Giggenbach, W.F., Garcia, P.N., Londono, C.A., Rodriguez, V.L., Rojas, G.N., and Calcache, V.M.L., 1990. The chemistry of fumarolic vapor and thermal-spring discharges from the Nevado del Ruiz volcanic-magmatic hydrothermal system, Columbia. *Jour. Volcanol. Geotherm. Res.*, v. 42, p. 13-39.

Giggenbach, W.F., and Soto, R.C., 1992. Isotopic and chemical composition of water and steam discharges from volcanic-magmatic-hydrothermal systems of the Guanacaste Geothermal Province, Costa Rica. *Applied Geochem.*, v. 7, p. 309-322.

Goldfarb, R.J., Leach, D.L., and Pickthorn, W.J., 1988. Application of fluid inclusion and stable isotope techniques to the study of Tertiary mesothermal gold deposits, Southern Alaska, U.S.A., *In: Bicentennial Gold '88*, Geol. Soc. Aust. Abstr., v. 23, p. 439-441.

Harley, M., 1993. The geology of the Sabie-Pilgrim's Rest goldfield with special reference to the Elandshoogte Mine. Unpub. Ph.D thesis, Univ. Witwatersrand, Johannesburg, 271 pp.

Harley, M., and Charlesworth, E.G., 1991. The mineralisation and structure of the Elandshoogte Gold Mine, Sabie-Pilgrim's Rest Goldfield, eastern Transvaal, South Africa, *in* Ladeira, E.A., (Ed.), Brazil Gold '91, Balkema, p. 685-692.

Harley, M., and Charlesworth, E.G., 1992. Thrust-controlled gold mineralization at the Elandshoogte Mine, Sabie-Pilgrim's Rest goldfield, South Africa. *Mineralium Deposita*, v. 27, p. 122-128.

Harley, M., and Charlesworth, E.G., 1993. The role of fluid pressure in the formation of bedding parallel, thrust-hosted gold deposits, Sabie-Pilgrim's Rest Goldfield, eastern Transvaal: Precamb. Res. Inform Circ. Econ. Geol. Res. Unit, Univ. Witwatersrand, Johannesburg, 264 (in press).

Hayashi, K.-I., and Ohmoto, H., 1991. Solubility of gold in NaCl- and H₂S-bearing aqueous solutions at 250-350°C. *Geochim. Cosmochim. Acta*, v. 55, p. 2111-2126.

Heald, P., Foley, N.K., and Hayba, D.O., 1987. Comparative anatomy of volcanic-hosted epithermal deposits: Acid-sulfate and adularia-sericite types: *Econ. Geol.*, v. 82, p. 1-26.

Helgeson, H.C., and Aagaard, P., 1985. Activity/composition relations among silicates and aqueous solutions: I. Thermodynamics of intrasite mixing and substitutional order/disorder in minerals. *American Jour. Science*, v. 285, p. 769-844.

Henley, R.W., 1973, The solubility of gold in hydrothermal chloride solutions. *Chem. Geol.*, v. 11, p. 622-635.

Holloway, J.R., 1981. Compositions and volumes of supercritical fluids in the earth's crust. *In: Hollister, L.S., and Crawford, M.L., (Eds.), MAC Short Course in Fluid Inclusions, Mineralogical Assoc. Canada, v. 6, p. 13-38.*

Holloway, J.R., 1984. Graphite-CH₄-H₂O-CO₂ equilibria at low-grade metamorphic conditions. *Geology*, v. 12, p. 455-458.

Jacobs, G.K., and Kerrick, D.M., 1981. Methane: an equation of state with application to the ternary system H₂O-CO₂-CH₄: *Geochim. Cosmochim. Acta*, v. 45, p. 607-614.

Jahn, B., Bertrand-Sarfati, J., Morin, N., and Macé, J., 1990. Direct dating of stromatolitic carbonates from the Schmidtsdrif Formation (Transvaal Dolomite), South Africa, with implications on the age of the Venterdorp Supergroup. *Geology*, v. 18, p. 1211-1214.

Johnson, J.W., Oelkers, E.H., and Helgeson, H.C., 1992. SUPCRT92: A software package for calculating the Standard Molal Thermodynamic Properties of minerals, gases, aqueous species, and reactions from 1 to 5000 bars and 0° to 1000°C. *Computers and Geosciences*, v. 18, p. 899-947.

Jones, H.D., and Kesler, S.E., 1992. Fluid inclusion gas chemistry in east Tennessee Mississippi Valley-type districts: evidence for immiscibility and implications for depositional mechanism *Geochim. Cosmochim. Acta*, v. 55, p. 137-154.

Kerrick, R., 1987. The stable isotope geochemistry of Au-Ag vein deposits in metamorphic rocks. *Mineral. Assoc. Canada Short Course Handbook*, v. 13, p. 287-336.

Kesler, S.E., Jones, H.D., and Arehart, G.B., 1991. Significance of O₂ and SO₂ in fluid inclusion analyses to hydrothermal geochemistry. *Geol. Assoc. Canada Program with Abstracts*, v. 16, p. A65.

Kishima, N., and Sakai, H., 1980. Oxygen-18 and deuterium determination on a single water sample of a few milligrams: *Anal. Chem.*, v. 52, p. 356-358.

Klein, C., and Beukes, N.J., 1990. Geochemistry and sedimentology of a facies transition from limestone to iron-formation deposition in the Early Proterozoic Transvaal Supergroup, South Africa *Econ. Geol.*, v. 84, p. 1733-1774.

Knipe, S.W., Foster, R.P., and Stanley, C.J., 1992. Role of sulphide surfaces in sorption of precious metals from hydrothermal fluids: *Trans. Instn Min. Metall. (Sect. B: Appl. Earth Sci.)*, v. 101, p. B83-B88.

Kretschmar, U. and Scott, S.D., 1976. Phase relations involving arsenopyrite in the system Fe-As-S and their application. *Can. Mineralogist*, v. 14, p. 364-386.

Kyser, T.K., 1987. Equilibrium fractionation factors for stable isotopes. In: Kyser, T.K. (Ed.), *Stable Isotope Chemistry of Low Temperature Fluids*: Min. Assoc. Canada Short Course, v. 13, p. 1-84.

Kyser, T.K., and Kerrich, R., 1990. Geochemistry of fluids in tectonically active crustal regions. *Mineralog. Assoc. Canada Short Course Handbook*, v. 18, p. 133-230.

Landis, G.P., and Rye, R.O., 1989. Reconnaissance gas chemistry of the Creede, Colorado, hydrothermal system. *U.S. Geol. Surv. Open-File Rept.*, v. 89-94, 51 pp.

Matsuhsia, Y., Goldsmith, J.R., and Clayton, R.N., 1979. Oxygen isotope fractionation in the system quartz-albite-anorthite-water: *Geochim. Cosmochim. Acta*, v. 43, p. 1131-1140.

Meyer, F.M., Welke, H.J., and Robb, L.J., 1986. Mineralogical and chemical characteristics of flat reefs in the Sabie-Pilgrim's Rest Goldfield. In: *Geocongress '86*, Johannesburg, Geol. Soc. S. Afr., p. 535-540.

Neal, F.B., 1987. Sulphidation of iron rich rocks as a precipitation mechanism for large Archaean gold deposits in Western Australia; thermodynamic confirmation. *In: Ho, S.E. and Groves, D.I., (Eds.), Recent Advances in Understanding Precambrian Gold Deposits.* Geol. Dept. Univ. Extension Univ. W.A. Pub. 11, p. 265-269.

Ohmoto, H., 1986, Stable isotope geochemistry of ore deposits, *in: Valley, J.W., et al., (Eds.), Stable Isotopes in High Temperature Geological Processes, Rev. Mineral.*, v. 16, p. 491-559.

Ohmoto, H., and Rye, R.O., 1979. Isotopes of sulfur and carbon. *In: Barnes, H.L., (Ed.), Geochemistry of Hydrothermal Ore Deposits.* Wiley Intersci., New York, p. 509-567.

Patterson, D.J., Ohmoto, H. and Solomon, M., 1981. Geologic setting and genesis of cassiterite-sulfide mineralization at Renison Bell, Western Tasmania: Econ. Geol., v. 76, p. 393-438.

Peters, S.G., 1993. Nomenclature, concepts and classification of oreshoots in vein deposits. *Ore Geol. Rev.*, v. 8, p. 3-22.

Potts, P.J., 1987. A Handbook of Silicate Rock Analysis: Blackie, London, 622 pp.

Robb, L.J., Anhaeusser, C.R., and Van Nierop, D.A., 1983. The recognition of the Nelspruit batholith north of the Barberton greenstone belt and its significance in terms of Archaean crustal evolution. *Spec. Publ. Geol. Soc. S. Afr.*, v. 9, p. 117-130.

Roedder, E., 1984. Fluid Inclusions. *Rev. Mineralogy*, v. 12, 644 p.

Roedder, E., 1990. Fluid inclusion analysis - Prologue and epilogue: *Geochim. Cosmochim. Acta*, v. 54, p. 495-507.

Roedder, E., and Bodnar, R.J., 1980. Geologic pressure determinations from fluid inclusion studies. *Ann. Rev. Earth Planet. Sci.*, v. 8, p. 263-301.

- Schidlowski, M., Eichmann, R., and Junge, C.E., 1975. Precambrian sedimentary carbonates: carbon and oxygen isotope geochemistry and implications for the terrestrial oxygen budget. *Precambrian Res.* v.2, p. 1-69.
- Schoonen, M.A.A., Fisher, N.S., and Wente, M., 1992. Gold sorption onto pyrite and goethite: A radiotracer study: *Geochim. Cosmochim. Acta*, v. 56, p. 1801-1814.
- Seward, T.M., 1973. Thio complexes of gold and the transport of gold in hydrothermal ore solutions. *Geochim. Cosmochim. Acta*, v. 37, p. 370-399.
- Sharp, Z.D. 1990. A laser-based microanalytical method for the in situ determination of oxygen isotope ratios in silicates and oxides. *Geochim. Cosmochim. Acta* v.54, p. 1353-1357.
- Sharpe, M.R., 1984. Petrography, classification and chronology of mafic sill intrusions beneath the eastern Bushveld Complex. *Bull. Geol. Surv. S. Afr.*, v. 77.
- Shenberger, D.M., and Barnes, H.L., 1989. Solubility of gold in aqueous sulfide solutions from 150 to 350°C. *Geochim. Cosmochim. Acta*, v. 53, p. 269-278.
- Sternner, S.M., and Bodnar, R.J., 1984. Synthetic fluid inclusions in natural quartz I: Compositional types synthesized and applications to experimental petrology. *Geochim. Cosmochim. Acta*, v. 48, p. 2659-2668.
- Swiegers, J.U., 1949. The gold deposits of the Pilgrim's Rest gold mining district, Transvaal. *Trans. and Proc. of the Geol. Soc. of S. Afr.*, v. 51, p. 81-132.
- Taylor H.P., 1979. Oxygen and hydrogen isotope relationships in hydrothermal mineral deposits, *In: Barnes, H.L., (Ed.), Geochemistry of Hydrothermal Ore Deposits: Wiley Intersci., New York*, p. 236-277.

Tyler, R., 1989. Cyclic sedimentation and gold mineralization in the Malmani Dolomite Subgroup, Pilgrim's Rest-Sabie area, Eastern Transvaal: Unpub. MSc. thesis, Univ. Witwatersrand, Johannesburg, 145 pp.

Vennemann, T.W., and O'Neil, J.R., 1993. A simple and inexpensive method of hydrogen isotope and water analyses of minerals and rocks based on zinc reagent. *Chem. Geol. (Isotope Geoscience Sect.)*, v. 103, p. 227-234.

Walraven, F., 1988. Notes on the age and genetic relationships of the Makhutso Granite, Bushveld Complex, South Africa. *Chem. Geol. (Isotope Geoscience Sect.)*, v. 72, p. 17-28.

Walraven, F., Armstrong, R.A., and Kruger, F.J., 1990. A chronological framework for the middle to late Precambrian stratigraphy of the Transvaal, South Africa. *Tectonophysics*, v. 171, p. 23-48.

Walsh, J.F, Kesler, S.E., Duff, D., and Cloke, P.L., 1988. Fluid inclusion geochemistry of high-grade, vein-hosted gold ore at the Pamour Mine, Porcupine Camp, Ontario: *Econ. Geol.*, v. 83, p. 1347-1367.

Walton, L.A., 1987. Geology and geochemistry of the Venus Au-Ag-Pb-Zn vein deposit, Yukon Territory. Unpubl. M.Sc. thesis, Edmonton, Univ. Alberta, 113 p.

Weir, R.H., Jr., and Kerrick, D.M., 1987. Mineralogic, fluid inclusion, and stable isotope studies of several gold mines in the Mother Lode, Tuolumne and Mariposa counties, California: *Econ. Geol.*, v. 82, p. 328-344.

Wybergh, W.J., 1925. The economic geology of Sabie and Pilgrims Rest. *Geol. Surv. Mem.* v. 23.

Zietsman, A.L., 1967. The relationship between mineralisation and structure in the Pilgrim's Rest - Sabie Goldfield: Unpubl. Ph.D thesis, Univ. Orange Free State, Bloemfontein, 198 pp.